RSC Advances

RSC Publishing

REVIEW

Nanostructured TiO_2 for energy conversion and storage

Cite this: *RSC Adv.*, 2013, **3**, 24758

Zhengyang Weng,[a] Huan Guo,[a] Xiangmei Liu,[a] Shuilin Wu,*[ab] K. W. K. Yeung[cd] and Paul. K. Chu*[b]

Received 31st July 2013
Accepted 13th September 2013

DOI: 10.1039/c3ra44031a

www.rsc.org/advances

Nanostructured TiO_2 possesses unique optical and physical properties as well as exhibiting quantum confinement effects and has attracted much attention in energy conversion and storage research. The energy related applications of nanostructured TiO_2 can be grouped into four main categories: lithium-ion batteries, dye-sensitized solar cells (DSSCs), fuel cells, and super-capacitors. Nanostructured TiO_2 with high crystallinity and/or a porous structure exhibits enhanced electron or ion transfer properties, enabling the fast diffusion of electrolytes, and consequently electrochemical processes proceed with high efficiency due to accelerated molecular adsorption. Its unique optical properties lead to improved photovoltaic performance and its bifunctional mechanism produces anti-poisoning effects on catalysts. This review discusses recent scientific and technological advances of nanostructured TiO_2 from the perspectives of energy conversion and storage.

1. Introduction

Titanium dioxide (TiO_2) has attracted much attention since the discovery of its excellent photocatalytic performance in water splitting when illuminated by ultraviolet (UV) light.[1–3] Subsequent development has spurred applications in environmental protection such as air purification[4,5] as well as for energy conversion devices like solar cells.[6,7] In 1991, O'Regan and Gratzel developed a low-lost and high-efficiency solar cell with a 10 μm thick and optically transparent film composed of nanoscale titanium dioxide particles.[8] Since then, there has been extensive research into the energy applications of nanostructured titanium dioxide.[9–12] Because the physical and chemical properties change as the size of a titanium dioxide particle shrinks to the nanometer scale, nanostructured TiO_2 exhibits the following advantages: photochemical stability, high catalytic efficiency, strong oxidation ability, and nontoxicity.[13–20] In addition, owing to the strong surface, volume, quantum, and macroscopic quantum tunneling effects, nanostructured TiO_2 delivers unique performance in acoustic, optical, electrical, magnetic, thermal, and other applications.[21] In particular, energy conversion and storage involve physical interactions and/or chemical reactions at the interface. In TiO_2, which is typically an n-type semiconductor, current can be generated when a photon stimulates the injection of an electron into the conduction band. The movement of electrons and holes is determined by quantum confinement, and hence, the photons are affected by the size and geometry of the materials.[10–12] Consequently, the surface area, energy, and chemistry play important roles in energy conversion, and as such, nanostructured TiO_2 offers many advantages favoring heat and charge transfer as well as accommodating the dimensional changes associated with chemical reactions and phase transitions. For example, a large surface area provides more sites for charge recombination in DSSCs[22,23] and smaller pores limit the penetration of electrolytes in supercapacitors.[24,25] Energy conversion or storage devices made of these materials can be produced by facile and controllable processes without secondary pollution.[26–30] The applications of nanostructured TiO_2 fall into four categories: lithium-ion batteries,[31–35] DSSCs,[36–41] fuel cells,[42–44] and supercapacitors.[45,46] In this paper, recent progress in the fabrication and application of nanostructured TiO_2 in energy conversion and storage is reviewed and various factors affecting the conversion efficiency are discussed.

[a]*Hubei Collaborative Innovation Center for Advanced Organic Chemical Materials, Ministry-of-Education Key Laboratory for the Green Preparation and Application of Functional Materials, Hubei Province Key Laboratory of Industrial Biotechnology, Faculty of Materials Science & Engineering, Hubei University, Wuhan 430062, China. E-mail: shuilin.wu@gmail.com; Fax: +86-27-88665610; Tel: +86-27-88661729*

[b]*Department of Physics & Materials Science, City University of Hong Kong, Tat Chee Avenue, Kowloon, Hong Kong, China. E-mail: paul.chu@cityu.edu.hk; Fax: +85-2-34420542; Tel: +85-2-34427724*

[c]*Division of Spine Surgery, Department of Orthopaedics & Traumatology, Li Ka Shing Faculty of Medicine, The University of Hong Kong, Pokfulam, Hong Kong, China*

[d]*Shenzhen Key Laboratory for Innovative Technology in Orthopaedic Trauma, The University of Hong Kong Shenzhen Hospital, 1 Haiyuan 1st Road, Futian District, Shenzhen, China*

2. Nanostructured TiO_2 in lithium ion batteries

2.1 Introduction to lithium ion batteries

Lithium-ion batteries (LIBs) are promising energy storage devices in mobile electronics, electric cars, and renewable energy systems operating on intermittent energy sources such

as wind and photovoltaics.[47] A lithium-ion battery consists of three major components: anode, cathode, and electrolyte. The device functions by converting a chemical potential into electrical energy *via* Faradaic reactions, which include heterogeneous charge transfer on the surface of the electrode. These reactions are accompanied by mass and charge transfer in the electrodes as well as dimensional variation, and the surface area and migration distance are critical parameters for determining the battery's performance. The composition, crystal structure, and morphology of the electrodes influence the reaction rate and transfer processes and can be manipulated to alter the overall electrochemical performance.[48]

The active cathode and anode materials in a typical LIB are $LiCoO_2$ and graphite respectively (Fig. 1).[49] They are electrically insulated by a porous polypropylene membrane and an intervening electrolyte of $LiPF_6$ in a mixture of organic solvents (*e.g.* ethylene carbonate and diethyl carbonate). During discharge, the potential difference between the anode and cathode drives the Li^+ ions from the anode to the cathode internally through the electrolyte. The reverse process occurs during charging.[50] The reversibility of the charging and discharging reactions on the electrodes determines the efficacy of the battery. The important performance indicators are capacity, cyclability, and rate capability, which depend on the properties of the active electrode materials. Research and development of economical and efficient energy-storage materials is a hot topic and nanostructured TiO_2 has attracted immense interest in this respect.[51]

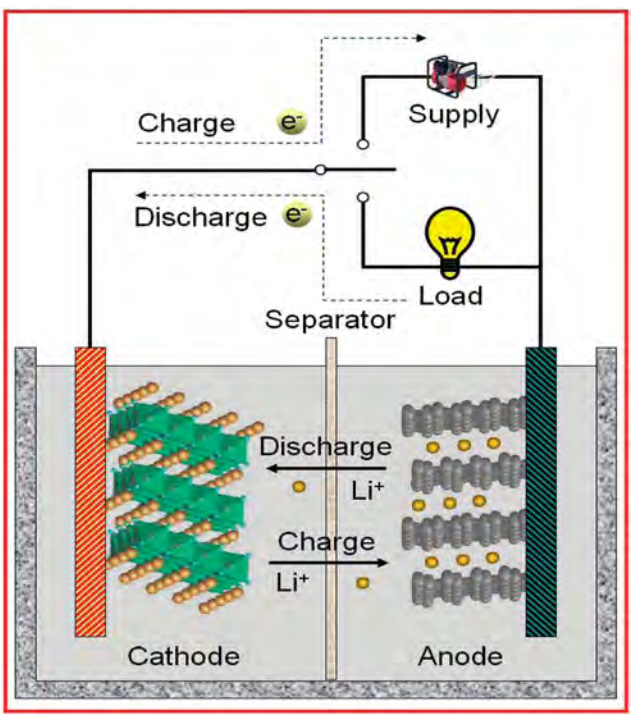

Fig. 1 Constituents of a typical lithium-ion battery and the electrochemical charging and discharging processes with the typical cathode and anode materials being $LiCoO_2$ and graphite, respectively. Reprinted with permission from ref. 49.

2.2 Nanostructured TiO_2-based Li-ion batteries

Considering the safety concerning overcharging and the stable voltage plateau at 1.78 V, anatase TiO_2, a typical Li-ion intercalation compound, is often used as the negative electrode in Li-ion batteries. The following typical lithium intercalation–deintercalation reaction occurs during the electrochemical process on the TiO_2 anode:

$$TiO_2 + XLi^+ + Xe^- = Li_XTiO_2, (0 \leq X \leq 1) \quad (1)$$

Unfortunately, low electrical conductivity, poor rate capability, and poor cycling performance can be induced by structural changes in the bulk materials during the lithiation process. However, nanostructured TiO_2 materials such as nanotubes, nanowires, nanorods, and nanoparticles can be used to overcome some of the drawbacks of the bulk materials.[52–57] Nanostructures with proper size and morphology can enhance the performance of a Li-ion battery, especially in reversible Li ion storage.[58] This is because the distance over which Li ions must diffuse in the solid state can be reduced and in comparison with conventional bulk electrodes, the current density in nanostructured TiO_2 electrodes is more effective due to their larger surface area.[59,60]

2.3 Factors affecting TiO_2-based LIB performance

Because of its excellent rate capability, good safety, environmental friendliness, and low cost,[61–68] nanostructured TiO_2 has attracted extensive interest as a potential anode material in high performance LIBs.[68] Recently, much attention has been paid to Li insertion, because nanostructured TiO_2 not only favors Li ion insertion/extraction at low voltage but it also expedites the process. The anodes are electrochemically stable and not easily passivated upon exposure to a liquid electrolyte in high-power lithium-ion batteries.[69–73] However, the morphology and structure of TiO_2 affect the electrochemical performance of lithium-ion batteries and these factors are discussed in the following sections.

2.3.1 TiO_2 particle size. The size effect of TiO_2 on electrochemical cycling in lithium-ion batteries has been studied. As the particle size diminishes, the Li storage capability increases due to the larger surface area.[74] For example, the discharge capacity of a rutile material with an average particle size of 300 nm (R300) is only 110 mA h g^{-1}, but 378 and 338 mA h g^{-1} are achieved from particles with sizes of 15 nm (R15) and 30 nm (R30), respectively. As shown in Fig. 2, in the R15 rutile electrode, 0.6–0.7 (the Li insertion ratio, Li : Ti) of the Li can be cycled reversibly and the discharging capacities are 132 and 118 mA h g^{-1} after 100 cycles at 5 and 10 A g^{-1}, respectively,[74] indicating that the rutile nanoelectrode has a high rate capability.

Hu *et al.* have indicated that nanometer-sized rutile materials have a higher electroactivity in Li insertion than their micrometer-sized counterparts.[75] The electrochemical behaviors of rutile materials with different particle size and shape are illustrated in Fig. 3a. At room temperature, for the rutile materials with an average diameter of 10 nm and length of

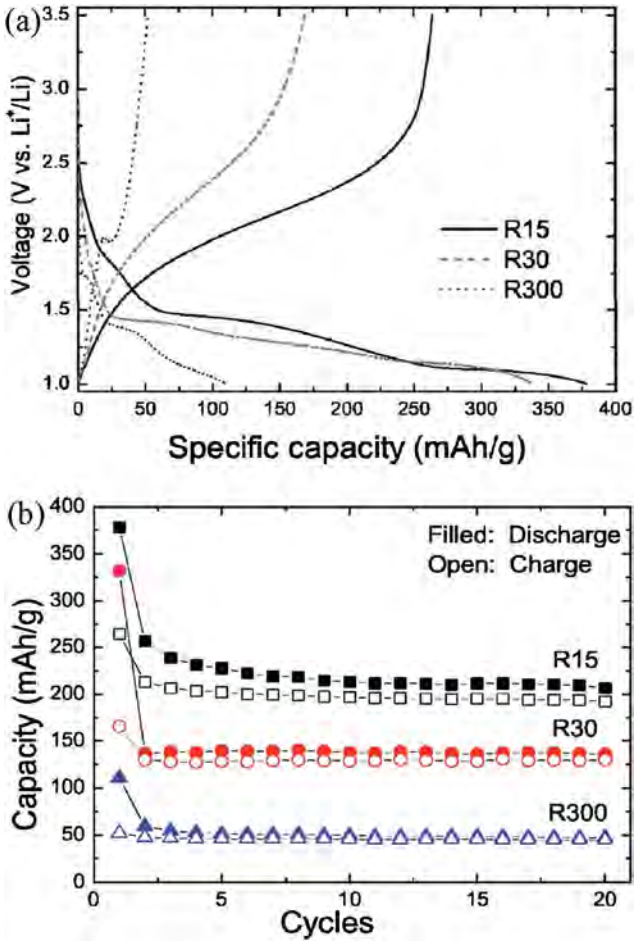

Fig. 2 (a) Voltage profiles of rutile TiO_2 with different particle sizes (R15, R30, and R300 denote particle sizes of 15 nm, 30 nm, and 300 nm) and (b) capacity *versus* cycle number in coin-type half cells at a rate of 0.05 A g^{-1}. Reprinted with permission from ref. 74.

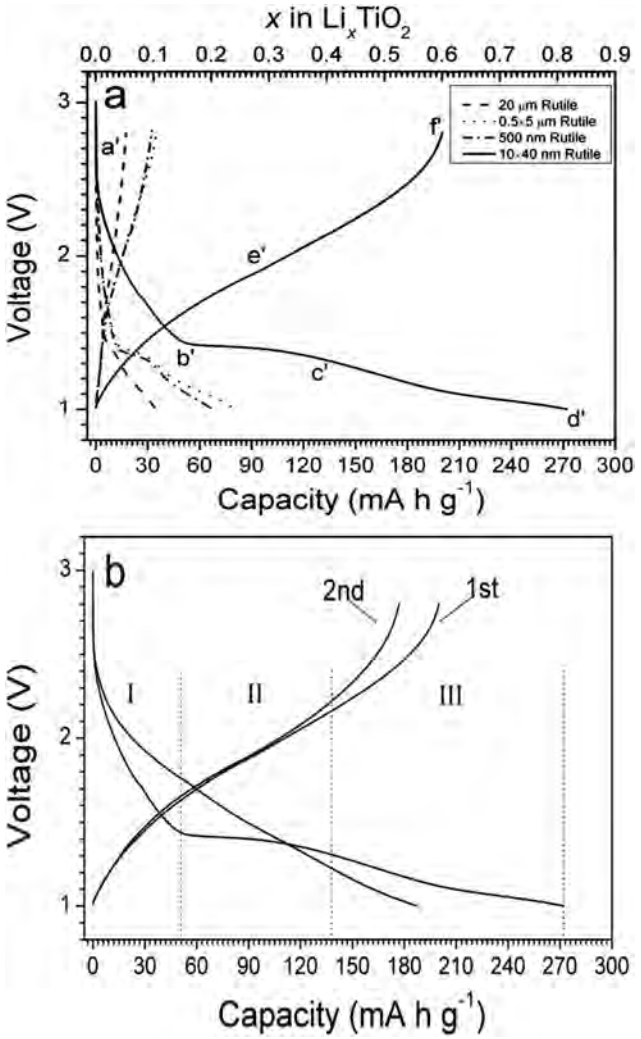

Fig. 3 (a) Voltage profiles of rutile electrodes of different particle size and shape cycled at a rate of C/20 between 1 and 2.8 V. The letters designate different Li insertion/extraction levels. (b) The first two cycles between the voltage limits of 1 and 2.8 V of the nanometer-sized rutile. Reprinted with permission from ref. 75.

30–40 nm, up to 0.8 mol of Li can be inserted in the first discharging process and about 0.5 mol of Li can be reversibly inserted/extracted in the subsequent discharging/charging processes. In contrast, only 0.1–0.25 mol of Li can be inserted in the micrometer-sized rutile structure.[75] This can be ascribed to slow Li diffusion along the *ab*-plane of the micrometer-sized rutile structure due to kinetic restrictions. The first discharge curve acquired from the nanometer-sized rutile materials can be divided into three regions. As shown in Fig. 3b, the voltage decreases gradually from 2.4 to 1.45 V in the first region, which is linked to the thermodynamically preferred surface storage of 0.15 mol of Li due to the reduced particle and crystallite size. In region II, a narrow plateau appears at 1.4 V corresponding to 0.35 mol of Li insertion. In region III, further Li insertion results in the formation of small crystal grains, which do not change significantly during the subsequent charging process.

In comparison with the bulk or macro/micrometer-sized materials, nanometer-sized rutile TiO_2 possesses excellent cycling capacity and high rate performance, thereby making it suitable for use as the anode in high-power LIBs. There are two reasons for the excellent high rate performance.[59,60,74,75] The short Li^+ diffusion length and increased specific surface area are obvious factors. In a short discharge–charge time, the diffusion length is the predominant factor determining the Li^+ insertion efficiency at high current rates, and a large surface area enhances the storage efficiency. Another possible reason is that because of the large surface area of the nanostructured materials, the small specific current density may also lead to a high rate performance.[70]

2.3.2 TiO_2 structure and morphology. Besides the particle size, the structure and morphology of the nanostructured TiO_2 influence the electrochemical performance of LIBs, altering the Li insertion capacity, electrochemical stability, and rate capability.[76–81] Mesoporous TiO_2 has been shown to be a suitable Li insertion electrode material because it can improve the cycling life, rate capability, and high power density of LIBs.[77] Wang *et al.* have developed a low-temperature approach to produce highly crystalline mesoporous rutile TiO_2 comprising mainly of interconnected rutile nanorods aligned along the [001] direction.[77] Their results show that mesoporous rutile TiO_2 with a

pore size varying from 2.2 to 3.8 nm has an excellent Li insertion activity (Fig. 4) and can accommodate up to $Li_{0.7}TiO_2$ during the first discharging step and $Li_{0.63}TiO_2$ in the second discharging step. Up to 0.55 Li ($Li_{0.55}TiO_2$, 185 mA h g^{-1}) can be charged and discharged reversibly at a rate of C/5 in the subsequent cycles with excellent capacity retention. The advantage of this mesoporous crystalline rutile structure is that the capacity is retained well with less than 10% capacity loss even after more than 100 cycles. Meanwhile, its mesoporous structure remains stable over the Li^+ insertion cycles.

Hierarchical nanostructured rutile TiO_2 has been reported to deliver enhanced LIB performance.[64,78] Using oxalic acid and $TiOSO_4$ as reagents, Fei *et al.* have fabricated rutile titania submicroflowers and microspheres composed of nanorods, by a facile hydrothermal method.[78] In comparison with the hierarchical anatase spheres self-assembled from ultrathin TiO_2 nanosheets,[64] these materials have a similar discharge capacity and cycle stability at the 0.5 C discharge rate and lower discharge capacity at the 1 C discharge rate. Although Chen's work shows that electrodes made of 3 nm rutile titania exhibit long term cycle stability after over 300 cycles with a capacity loss of 0.17 per cycle and a good rate capability up to a 30 C rate, mainly due to there being more lithium insertion sites as a result of the large surface area and short diffusion path,[61] the hierarchical rutile microflowers comprising of nanorods have a large discharging capacity at a small discharging rate. That is to say that as well as by changing the nanoparticle size, the performance of LIBs can be adjusted by changing the hierarchical structure of the nanostructured TiO_2 because this change can lead to the efficient solid-state diffusion of Li^+ as a consequence of the small building blocks.[61,62,64,78]

By controlling the nano-TiO_2 shape the performance of LIBs can be enhanced, and consequently there has been much progress in the synthesis and application of TiO_2 nanoparticulates, nanotubes, nanofibers, nanowires, and nanobelts as electrodes.[79–86] These materials, which can be synthesized using a simple aqueous technique or electrospinning with a high yield, have diameters of 40 to 60 nm and lengths of up to several micrometers. The TiO_2-B polymorph is an excellent intercalation host for Li capable of accommodating up to $Li_{0.91}TiO_2$-B (305 mA h g^{-1}) at 1.5–1.6 V *vs.* Li^+(1 M)/Li and has excellent capacity retention on cycling. As shown by the charging and discharging curves of Li_xTiO_2-B nanowires at the rate of 10 mA g^{-1} in Fig. 5a, these nanowires have a much better rate capability than the nanoparticles (Fig. 5b).[79]

Nie *et al.* have adopted a hydrothermal method to synthesize one-dimensional TiO_2-B nanobelts,[80] which have a very high reversible intercalation–deintercalation lithium capacity of up to 265 mA h g^{-1}. A similar performance can be achieved from *c*-axis grown rutile TiO_2 nanorod array anodes.[81] Dong *et al.* have fabricated these materials on metallic titanium sheets hydrothermally[81] and shown that the reversible electric capacity can reach 133 μA h cm^{-2} after cycling for fifty times at 15 μA cm^{-1}. The electrical capacity is 10 times larger than that of the normal

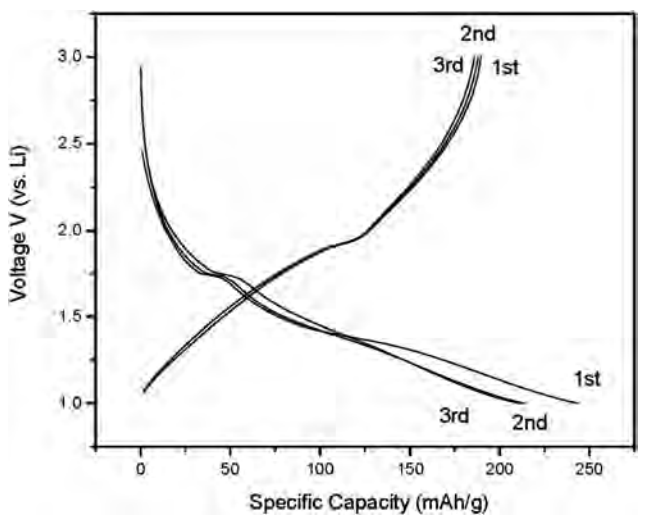

Fig. 4 First three potential–capacity profiles of mesoporous crystalline TiO_2 with $C_{12}H_{25}SO_4Na$ (MCT-12) as the surfactant template at a rate of C/5 between the voltage limits of 1 and 3 V *vs.* Li^+/Li. Reprinted with permission from ref. 77.

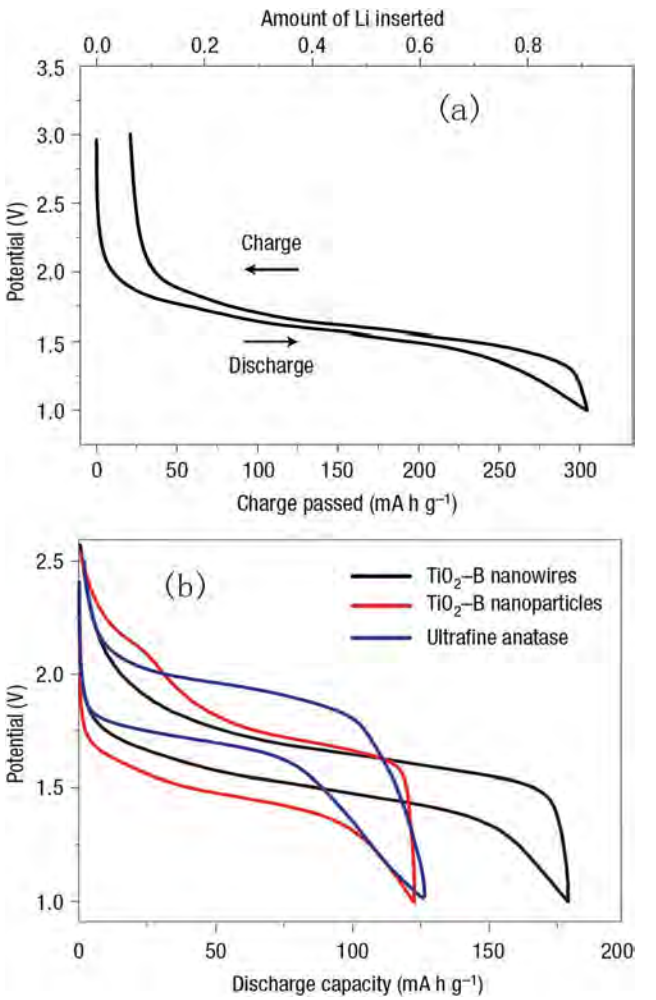

Fig. 5 Charging and discharging curves of the nanostructured anode materials: (a) charging and discharging curves of Li_xTiO_2-B nanowires (rate of 10 mA g^{-1}). (b) Comparison of the cycling behavior of TiO_2-B nanowires, TiO_2-B nanoparticles, and nanoparticulate anatase at 200 mA g^{-1}. Reprinted with permission from ref. 79.

TiO_2 anode, indicating that the nanorod array anode can effectively improve the performance of LIBs.

A simple electrospinning process encompassing post-nitriding has been employed to synthesize TiO_2 nanofibers with different structures.[83] The nitrided TiO_2 hollow nanofibers deliver a rate capability twice that of pristine TiO_2 nanofibers at 5 C, which is attributed to the shorter lithium ion diffusion length and high electronic conductivity along the surface of the nitrided hollow nanofibers.[83]

The different crystalline forms of titanium dioxide also affect the electrochemical performance of TiO_2-based LIBs. Ryu *et al.*'s results reveal that the amorphous TiO_2 nanotube electrodes have better rate capability than anatase nanotube electrodes.[84] They observe a higher discharge capability of 0.088 mA h cm^{-2} from the former compared to 0.047 mA h cm^{-2} for the latter. The difference in the rate capability between the two structures is ascribed to the better reversibility and higher Li^+ diffusivity of the former.[84]

Recent research also confirms that some structures enhance the electrochemical performance of TiO_2 electrodes.[85,86] For example, the calcined TiO_2 flakes (CF-TiO_2) prepared by Yang *et al.* possess a larger reversible charge–discharge capacity as well as a better rate capability and cycling stability than anatase TiO_2 nanoparticles.[85] The nano-sized grains in these flakes may eliminate the dual phases in a single particle during lithiation, thus improving the cycling performance significantly. The larger surface area provides a larger electrode–electrolyte contact area, shorter solid state path lengths for both Li^+ and electron transport, and eventually a better rate capability of the CF-TiO_2.[85] Fig. 6 shows the variation in the specific charge–discharge capacity with respect to the cycle number for CF-TiO_2 and TiO_2 nanoparticles at a constant current density (C/20).[85] The yolk–shell nano-architecture has recently been shown to improve the electrochemical performance of sulfur–TiO_2.[86] An initial specific capacity of 1030 mA h g^{-1} at 0.5 C and coulombic efficiency of 98.4% over 1000 cycles can be achieved from this electrode and the capacity decay after 1000 cycles is as small as 0.033% per cycle.[86] It is believed that the internal void accommodates the volume expansion caused by sulfur during lithiation, consequently producing a complete shell to minimize polysulfide dissolution.[86]

2.3.3 Doping. Doping control is important because the performance of electrode materials can be affected. The doping process can affect the electronic structure of TiO_2 altering the electronic,[87,88] optical,[89,90] photoelectrical,[91–93] and electrochemical performance.[94] The effects of aliovalent ions on the electrical conductivity are related to the concentration of the electronic charge carriers but the effect on mobility is insignificant.[95] Recent research shows that doped TiO_2 is a promising anode in lithium-ion batteries.[96–98] Nam *et al.* have prepared metal-nanoparticle-doped one-dimensional titanium dioxide nanofibers (1D-TiO_2) by a one-step electrospinning process, in which Au or Ag nanoparticles 5 to 10 nm in diameter are incorporated into the TiO_2 nanofibers.[97] Because of the altered crystallinity and size of TiO_2 in the Ag-doped 1D-TiO_2 and Au-doped 1D-TiO_2 nanofibers, Li^+ diffusion and charge transfer are promoted. In particular, the specific capacity of the electrodes made of the nanoparticle-doped 1D-TiO_2 nanofibers increases by at least 20% and the rate performance goes up by a factor of two compared to 1D-TiO_2.

A similar process has been adopted by Zhao *et al.* using carbon as the dopant.[98] By means of electrospinning, Zhao *et al.* have prepared a highly flexible self-standing thin-film electrode composed of mesoporous rutile TiO_2–C nanofibers with a low carbon content (<15 wt%). These materials, which can be used directly as electrodes in LIBs without further treatment, deliver outstanding electrochemical performance. As shown in Fig. 7, stable capacities of 122, 108, and 92 mA h g^{-1} can be reached at rates of 1, 2, and 5 C, respectively. A value of 70 mA h g^{-1} can be maintained even at a high rate of 10 C and the experimental results confirm that the mesoporous rutile TiO_2–C nanofibers have good electrochemical characteristics in lithium-ion batteries.[98] Wang *et al.* have incorporated carbon species into porous TiO_2 hollow shells using multiple sol–gel processes followed by carbonization.[99] The porous TiO_2–C

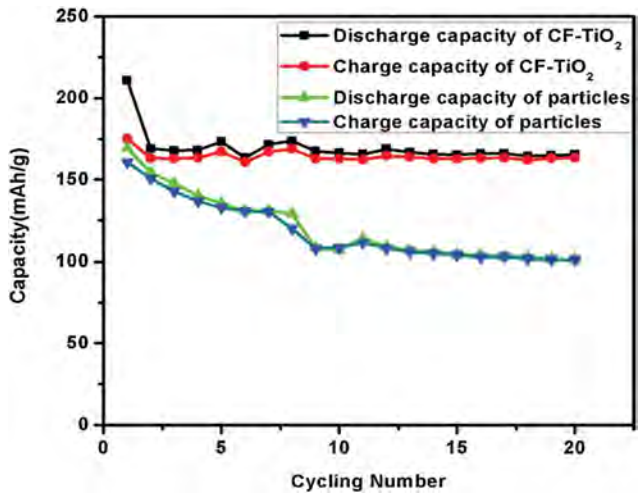

Fig. 6 The variation of specific discharge capacity with respect to the cycle number of CF-TiO_2 and nanoparticles. Reprinted with permission from ref. 85.

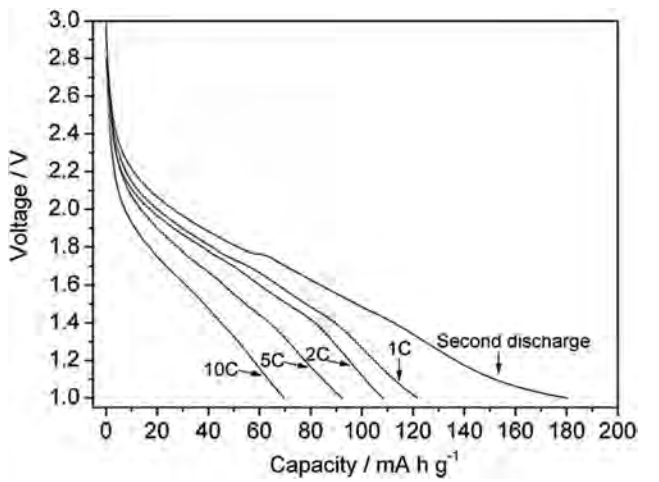

Fig. 7 Capability of the cells with the U-TiO_2 film electrode. Reprinted from ref. 92.

nanocomposites significantly improve the cycling performance in Li ion storage and rate capability up to 10 C.[99] Compounds have also been introduced into TiO_2 to form TiO_2 composites.[100–105] These composites including TiO_2–graphene nanocomposites,[101] mesoporous TiO_2–C–Cu composites,[102] nanoarchitectured TiO_2-B/ACF,[103] and FeS–TiO_2 nanostructured materials[104] enhance the storage rate of TiO_2-based LIBs by offering electrons to TiO_2.

Cai *et al.* have prepared TiO_2–graphene nanocomposites by a facile gas/liquid interface reaction.[101] The TiO_2–graphene nanocomposites are promising anode materials for LIBs boasting a high specific capacity and excellent rate performance. Fig. 8 presents the initial discharge–charge curves of the TiO_2–graphene nanocomposites and bare TiO_2 nanoparticles at a current density of 100 mA g^{-1} between 0.01 and 3.0 V. The specific charge capacity of the TiO_2–graphene nanocomposites is much larger than that of the bare TiO_2 nanoparticles due to the four following factors: (1) the lithium storage performance of graphene is obtained during the discharge–charge of the TiO_2–graphene nanocomposites between 0.01 and 3.0 V; (2) the graphene sheets prevent aggregation of TiO_2 nanoparticles; (3) graphene facilitates electron transfer; (4) the mesoporous structure can provide a large electrode–electrolyte contract area and short path length for both electron and Li-ion transport.[101]

The ordered mesoporous TiO_2–C composites embedded with Cu nanoparticles (TiO_2–C–Cu) have been prepared *via* an evaporation induced self-assembly method and *in situ* crystallization.[102] The TiO_2–C–Cu composites display promising lithium insertion/extraction characteristics as anode materials for LIBs. Fig. 9 shows the cycling performance of TiO_2–C and TiO_2–C–Cu at 0.5 C. The capacity of TiO_2–C decays more quickly than TiO_2–C–Cu after the 15th cycle. It is believed that Cu nanoparticles embedded in the composites improve the conductivity significantly and enhance the efficiency of Li^+ diffusion and the coulombic efficiency.[102]

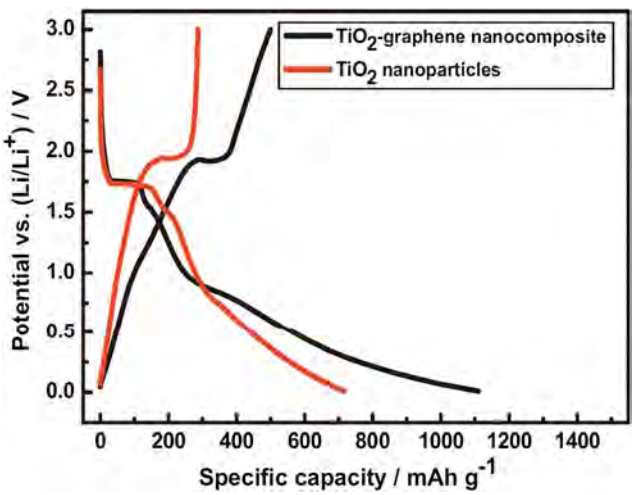

Fig. 8 The initial discharge–charge curves of a TiO_2–graphene nanocomposite and TiO_2 nanoparticles at a current density of 100 mA g^{-1} between 0.01 and 3.0 V. Reprinted with permission from ref. 101.

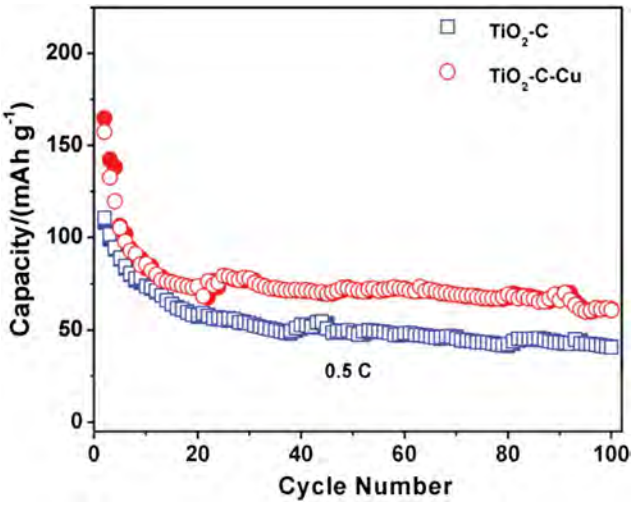

Fig. 9 Cycling performance at 0.5 C of TiO_2–C and TiO_2–C–Cu composites. Reprinted with permission from ref. 102.

An additive-free flexible film electrode (TiO_2-B/ACF) fabricated by anchoring TiO_2-B nanosheets on non-woven activated carbon fabric (ACF) has been reported by Liu *et al.*[103] The ultrathin TiO_2-B nanosheets expedite lithium storage due to intrinsic open channels, large surface area, and reduced diffusion length. The carbon nanofibers not only allow easy access for ions but also produce electrodes with good conductivity and high mechanical flexibility. As a result, the flexible binder free TiO_2-B/ACF electrodes have high reversible capacity, excellent rate capability, and superior long-term cycling stability.[103]

An electrode made of anatase TiO_2 modified FeS nanowires exhibits an improved reversible capacity of 510 mA h g^{-1} after 100 discharge–charge cycles at 200 mA g^{-1}, which is much larger than that of the pristine FeS nanostructure electrode.[104] Meanwhile, the FeS–TiO_2 electrode possesses enhanced rate capability and long-term cycling stability with little performance degradation. This superior electrochemical performance can be attributed to the incorporation of anatase TiO_2, which increases the conductivity of the integrated electrode and favors lithium insertion/extraction at the electrode/electrolyte interface as well as diffusion of lithium ions.[104]

2.4 Remarks

Based on the discussions above, nano-structured TiO_2 electrode materials improve the performance of lithium-ion batteries. The large surface area of nano-TiO_2 materials such as nanosheets and nanotubes enhances the cycling performance of LIBs as a result of better conduction, larger contact area between the materials and electrolyte, shorter Li^+ diffusion distance, and stable structure during charging and discharging. Future improvement pertaining to the control of the structure and doping process of TiO_2 nanomaterials will improve the conductive ability, lithium power, and cycle life. In summary, nano-TiO_2 will likely become the mainstream material in future high-performance lithium-ion batteries.

3. Nanostructured TiO_2 in dye-sensitized solar cells (DSSCs)

Solar energy is the preferred renewable energy source as the sun delivers to the earth 1.2×10^5 terawatts (TWs) of energy, which exceeds the current energy need of 13 TWs.[106] This translates into the idea that by covering only 0.1% of the earth's surface with solar cells with 10% efficiency, our energy needs will be satisfied.[107] However, solar energy currently constitutes far below 0.1% of the global energy demand (Fig. 10)[108] because of the major obstacles encountered in the production of large-scale solar materials, including cost and efficiency. It is necessary to develop new techniques to capture sunlight more effectively and produce photovoltaic materials more economically.[109,110] Since DSSCs are considered to be one of the major types of photovoltaic devices, improving the photoelectric conversion efficiency of DSSCs is of paramount importance.

3.1 Overview of DSSCs

DSSCs have been widely studied by researchers[111–115] and Fig. 11 schematically illustrates their structure and operating principles.[116] The heart of the device is the nanocrystalline mesoporous oxide film with a thickness of about 10 μm and porosity of 50–60%. It is often made of a network of TiO_2 nanoparticles with average diameters between 10 and 30 nm to establish electrical conduction. The mesoporous layer is typically deposited on a transparent conducting oxide (TCO) on a glass or plastic substrate and attached to the surface of the nanocrystalline film is a monolayer of the charge-transfer dye. Photoexcitation of the latter induces injection of electrons into the conduction band of the oxide keeping the dye in the oxidized state. The dye returns to the ground state *via* electron transfer from the electrolyte, which is usually an organic solvent containing a redox system such as the iodide/triiodide couple. During the regeneration of the sensitizer the iodide intercepts the recapture of the conduction band electron by the oxidized dye. The I_3^- ions formed by the oxidation of I^- diffuse over a short distance (<50 μm) through the electrolyte to the cathode that is coated with a thin layer of a platinum catalyst, where the regenerative cycle is completed by electron transfer to reduce I^{3-} to I^-.[116–119] The device converts light into electrical energy without a permanent chemical reaction.

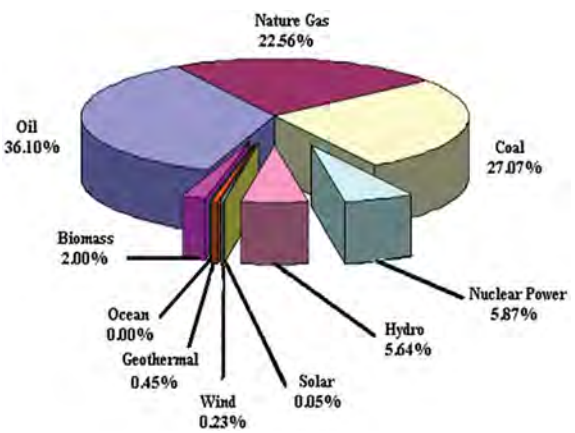

Fig. 10 Worldwide primary energy consumption by energy type. Reprinted with permission from ref. 108.

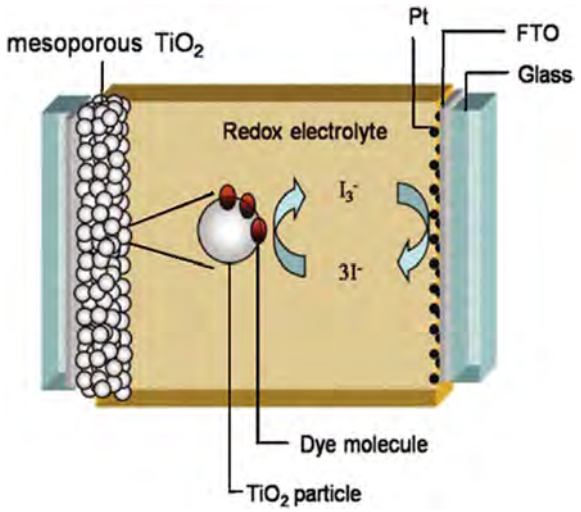

Fig. 11 Schematic overview of a dye-sensitized solar cell. Reprinted with permission from ref. 116.

3.2 Nano-TiO_2 in DSSCs

Owing to its large specific surface area, high efficiency, low cost, and flexibility, nanostructured TiO_2 holds high promise as an electrode in DSSCs. TiO_2 exists in various structures including anatase, rutile, and brookite.[120,121] The rutile form is the thermodynamically most stable phase while anatase is the preferred structure in DSSCs, because the bandgap of the latter is 3.2 eV, which is larger than that of rutile (3.0 eV). In addition, the latter has a larger conduction band edge energy than the former, thereby producing a higher Fermi level and V_{oc} for anatase in DSSCs for the same conduction band electron concentration.

Improvements in TiO_2 electrodes in DSSCs in terms of light absorption, light scattering, and charge transport, which control the charge recombination and enhance the interfacial energy, are being made. Advanced DSSCs typically employ a mesoporous TiO_2 electrode fabricated by the following process. A TiO_2 blocking layer (about 50 nm thick) is deposited on a transparent conducting oxide such as FTO (fluorine-doped tin oxide) to prevent direct contact between the redox mediator in the electrolyte and FTO.[122] A light absorption layer composed of a 10 μm thin film of mesoporous TiO_2 particles provides a large surface area for sensitizer adsorption and good electron transport to the substrate.[121] A light scattering layer is produced on top of the mesoporous film. It consists of a 3 μm thick porous layer consisting of 400 nm TiO_2 particles[123,124] and finally, an ultrathin overcoating of TiO_2 is deposited chemically.[114,115]

3.3 Factors influencing the conversion efficiency of DSSCs

3.3.1 Preparation processes. Substantial progress has been made recently in the synthesis of TiO_2 nanostructures using

methods such as sol–gel,[125–129] hydrothermal,[130–132] solvothermal,[133–135] sonochemical,[136,137] chemical vapor deposition,[138,139] and physical vapor deposition.[140,141] The conversion efficiency of the DSSCs depends on the fabrication process. Hore *et al.* have found that alkali-catalyzed conditions produce mesoporous TiO_2 with slower interfacial recombination and a higher open circuit voltage, but the quality of dye adsorption is reduced compared to the acid-catalyzed TiO_2.[142] This has been corroborated by Lee *et al.*[143] who have prepared two types of nano-TiO_2 by sol–gel and solvothermal methods. Their results show that the energy conversion efficiency of the TiO_2 modified by the latter method is approximately 8.51%, while the value for the former modified TiO_2 is only 5.93% under illumination of 100 mW cm^{-2} of simulated sunlight with N719 as the dye (Fig. 12).[143] Electrostatic force microscopy (EFM) reveals that the electrons are transferred more rapidly to the surface of the solvothermally modified TiO_2 film than the sol–gel modified TiO_2 film. This is due to the smaller particles, stronger absorption, and larger red-shift of the TiO_2 synthesized by the solvothermal process.

3.3.2 Structure. Nanostructured TiO_2 not only provides a large internal surface area to the photoelectrode film, but also gives rise to other functions enhancing optical absorption or electron transport.[144–146] Besides TiO_2 nanoparticles, many other nanostructures such as nanobelts, nanowires/nanorods, nanotubes, hierarchical micro–nanostructures, and core–shell structures of TiO_2 have been extensively studied. Nevertheless, the efficiency record of 11–12% for DSSCs is still held by nanocrystalline TiO_2 films.[147,148]

3.3.2.1 Morphology. The morphology of nanostructured TiO_2 affects the conversion efficiency. Dhas *et al.* have synthesized anatase TiO_2 nanoleaves (NLs) with a large surface area (~93 m^2 g^{-1}) hydrothermally,[149] and the performance of DSSCs made with the NLs has been compared to that made of hydrothermal TiO_2 nanoparticles (NPs) and Degussa P25 powder. The DSSCs composed of the NLs boast a higher conversion efficiency (~5.6%) than those made of NPs (~4.8%) and P25 (~4.5%). The highest efficiency (~6.5%) is achieved from DSSCs composed of mixed NLs and NPs with a ratio of 50 : 50 (Fig. 13).[149] In the NP and NL mixture, the dye loading was more than 50% greater than that for the NP films. Moreover, the DC resistance to diffusion of I_3^- in the electrolyte is substantially lower. These two aspects are believed to be responsible for the higher efficiency of the former.

3.3.2.2 Lengths of TiO_2 nanotubes (NTs). TiO_2 nanotube arrays are used in dye sensitized solar cells (DSSCs)[150] and a larger tube length can enhance both the short-circuit current density and conversion efficiency. The results are summarized in Fig. 14.[150] Pan *et al.* have recently produced a TiO_2 nanotube array with ~10 nm TiO_2 nanoparticles by infiltration with a

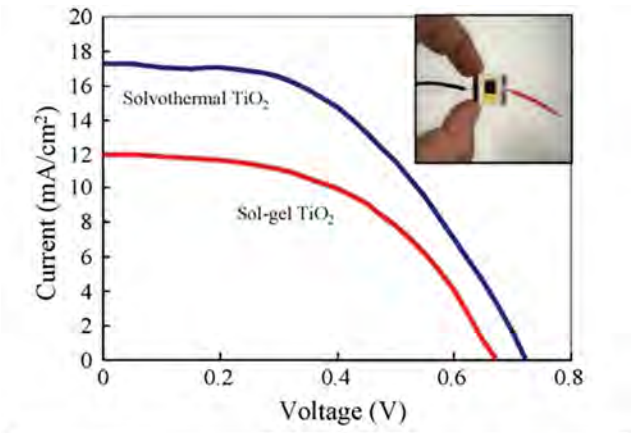

Working electrode	Dye	Efficiency(%)	Fill factor	Voc(V)	Jsc(mA/cm^2)
Sol-gel TiO_2	N719	5.93	0.68	0.73	11.95
Solvorthermal TiO_2	N719	8.51	0.65	0.76	17.23

Fig. 12 Solar energy conversion efficiency of the DSSCs fabricated with the two types of TiO_2 using conventional solvothermal and sol–gel methods. Reprinted with permission from ref. 143.

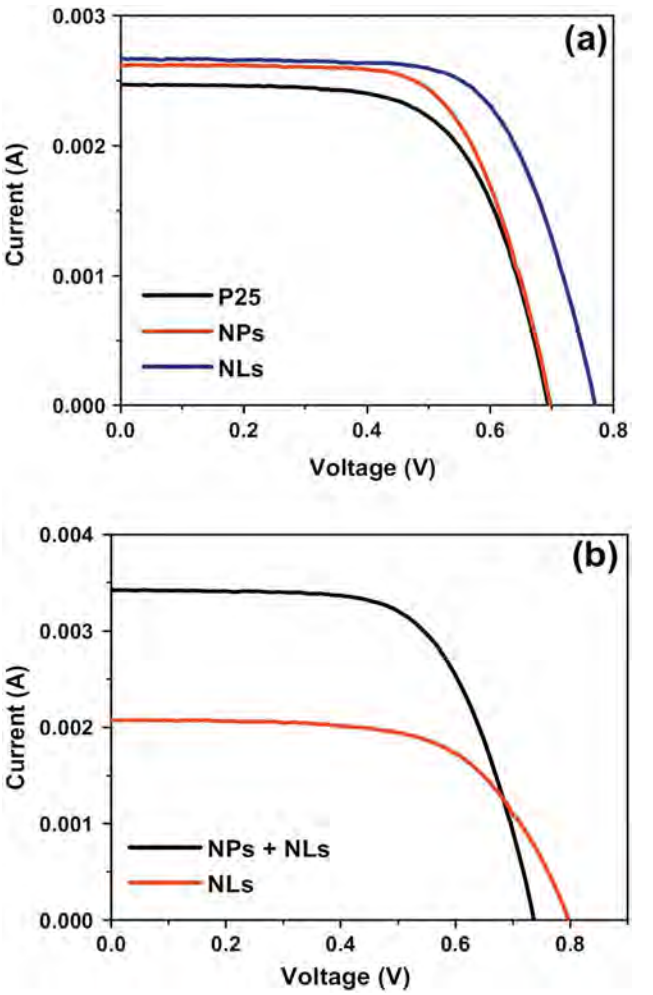

Fig. 13 (a) Comparison of solar cell characteristics between DSSCs composed of TiO_2 nanoleaves and those made of P25 and TiO_2 nanoparticles (film thickness = 12 μm). (b) Comparison of the solar cell characteristics between DSSCs composed of TiO_2 nanoparticles and the mixture of nanoparticles and nanoleaves (film thickness = 10 μm). Reprinted with permission from ref. 149.

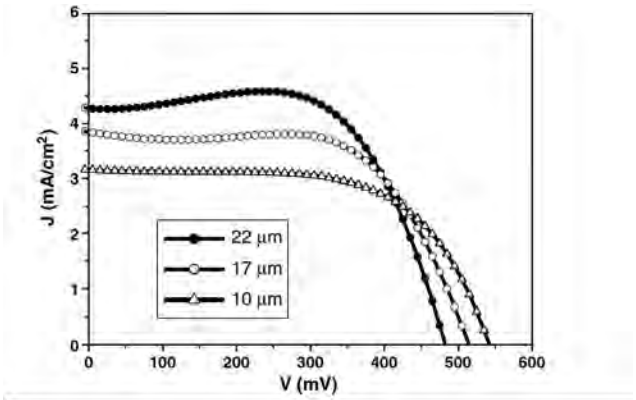

Length (μm)	Efficiency(%)	Fill factor	Voc(mV)	Jsc(mA/cm²)
10	1.08	0.629	541.48	3.16
17	1.25	0.631	514.50	3.85
22	1.39	0.672	482.91	4.29

Fig. 14 *I–V* characteristics of the DSSCs based on the TiO_2 nanotube arrays with different tube lengths. Reprinted with permission from ref. 150.

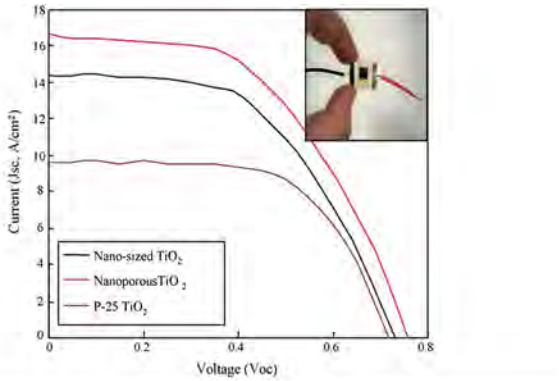

Working electrode	Dye	Efficiency(%)	Fill factor	Voc(mV)	Jsc(mA/cm²)
Nano-sized TiO_2	N719	7.03	0.68	0.72	14.36
Nanoporous TiO_2	N719	8.71	0.67	0.78	16.66
P-25 TiO_2	N719	4.23	0.62	0.71	9.60

Fig. 15 Photocurrent–voltage curves of the DSSCs fabricated with nano-sized and nanoporous TiO_2. Reprinted with permission from ref. 153.

$TiCl_4$ solution by a hydrothermal process.[151] Compared to DSSCs made of bare TiO_2 nanotubes, these mixed NT and NP structures (8 and 13 μm long) double the dye loading and boost the photocurrent by nearly 100%. This is because of the enhanced photovoltage and filling factor of the structure with a small serial resistance. The overall photon conversion efficiency of the DSSCs made of the NTs is improved by 152%, 107%, and 49% for 8, 13, and 20 μm long NTs, respectively, indicating that TiO_2 nanotubes that are too long are not optimal. This is attributed to the small electron collection efficiency induced by electron trapping during transport in the nanotubes.

3.3.2.3 Nanoporous structure. A high light-to-energy conversion efficiency has been achieved from DSSCs composed of nanoporous TiO_2 electrodes.[152] The key is to employ a mesoporous TiO_2 electrode, which has a large internal surface area supported by a monolayer of the sensitizer.[8] The device absorbs a large proportion of the solar energy (46%) and has an efficiency of over 80% for the conversion of photons to electrical current. The overall light-to-electric energy conversion yields are 7.1–7.9% for simulated solar light and 12% in diffuse daylight. There is strong evidence that the nanoporous TiO_2 electrode enhances the energy-conversion efficiency of the DSSCs device.[153] In comparison with nano-TiO_2, under 100 mW cm^{-2} simulated sunlight with N719 as the dye, the conversion efficiency of DSSCs made of nanoporous TiO_2 increases from 4.23% to 8.71% and the current density rises from 9.60 to 16.66 mA cm^{-2}, as shown in Fig. 15.[153] This can be explained by an adsorption mechanism. In the nanoporous structure, more dye molecules can be absorbed on the nanoporous structured TiO_2 than the nano-TiO_2 particles and so electrons can be transferred rapidly in the nanoporous TiO_2 film.

3.3.2.4 Core–shell structure. Core–shell TiO_2 electrodes can enhance the performance of DSSCs.[154–159] Their structure consists of nanoporous TiO_2 covered with a shell of another metal oxide, which possesses the ability to retard the recombination processes by forming an energy barrier at the TiO_2 surface.[154,155] The conduction band potential of this shell should be more negative than that of TiO_2 in order to generate an energy barrier for the reaction between the electrons in TiO_2 and the oxidized dye or the redox mediator in the electrolyte.[156–158]

There are two common techniques used to fabricate nanoporous TiO_2 core–shell electrodes.[160,161] The first process utilizes ZnO-covered nanocrystalline TiO_2 composed of TiO_2 cores and zinc oxide shells prepared by the addition of $Zn(CH_3COO)_2 \cdot 2H_2O$ into a TiO_2 colloid solution followed by annealing.[160] An energy barrier forms at the electrode/electrolyte interface and between the individual TiO_2 nanoparticles. The second approach involves nanoporous TiO_2 as the thin shell, which acts as an energy barrier at the electrode/electrolyte interface to slow the interaction between the electrons in the electrode and electrolyte ions to enhance the conversion efficiency by a factor of 2.2.[161]

In general, a well-defined core–shell configuration of a nanoporous electrode is usually made of a TiO_2 core coated with Nb_2O_5,[154] SiO_2,[159] ZrO_2,[159] Al_2O_3,[161–164] or MgO.[165] Zaban *et al.* have discovered that TiO_2–Nb_2O_5 nanoporous electrodes can improve the performance of DSSCs by over 35%.[154] A schematic diagram showing the bilayered nanoporous electrodes and the related *I–V* curves are depicted in Fig. 16A and B, respectively. The three types of core–shell electrodes show better *I–V* performance than the bare TiO_2 anode. By adopting optimized deposition conditions, the photocurrent increases from 10.2 to 11.4 mA cm^{-2} and the photovoltage rises from 661 to 730 mV, accompanied by an increase in the fill factor from 51.0 to 56.5%. As a result, the conversion efficiency of the solar cell increases by 35% from 3.62% to 4.97%.[154] The shell materials sometimes shift the conduction band potential of the core rather than forming an energy barrier. For example, a coating of TiO_2 with a

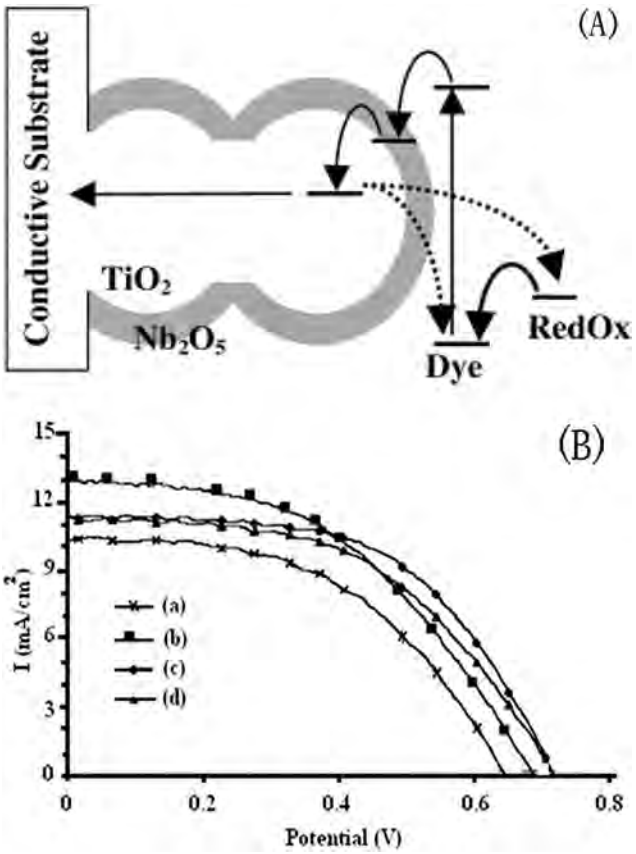

Fig. 16 (A) Schematic view of the new bilayered nanoporous electrode consisting of a nanoporous TiO_2 matrix covered with a thin layer of Nb_2O_5. The Nb_2O_5 coating forms an inherent energy barrier at the electrode/electrolyte interface to reduce the recombination rate of the photoinjected electrons. (B) *I–V* curves of four DSSCs with different nanoporous electrodes: (a) TiO_2 reference electrode and (b–d) three bilayer electrodes: (b) Nb_2O_5 coating made by the 30 s dipping of a 6 μm TiO_2 matrix in a 5 mM solution of: $NbCl_5$ in dry ethanol, (c) Nb-(isopropoxide)$_5$ in 2-propanol, and (d) Nb-(ethoxide)$_5$ in ethanol. Reprinted with permission from ref. 154.

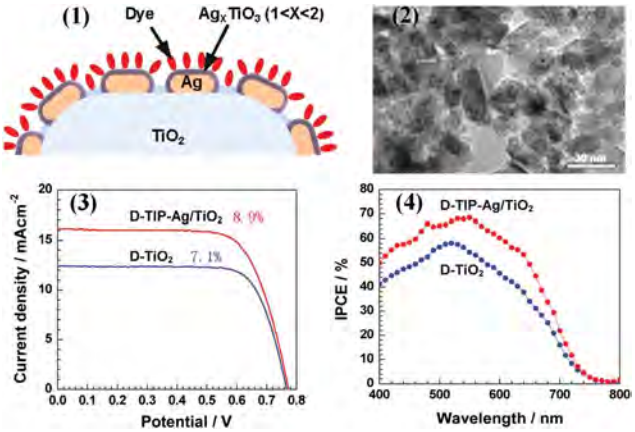

Fig. 17 Ag/TiO_2 in dye-sensitized solar cells: (1) schematic drawing showing the structure of the photoelectrode film consisting of Ag nanoparticle-coated TiO_2 sensitized by dye, (2) TEM image of Ag nanoparticles attached onto TiO_2 particles, (3) *I–V* curves, and (4) IPCE (incident photon-to-electron conversion efficiency) spectra of a dye-sensitized pure TiO_2 film (D-TiO_2) and dye-sensitized TiO_2 film with attached titanium isopropoxide treated Ag nanoparticles (D-TIP–Ag/TiO_2). Reprinted with permission from ref. 169.

$SrTiO_3$ shell produces a shift of the TiO_2 conduction band in the negative direction.[155,156] Growth of an overlayer of Al_2O_3 on a nanocrystalline TiO_2 film improves the DSSC performance. For instance, a 4-fold retardation of the interfacial charge recombination and 30% improvement in the photovoltaic device efficiency have been observed.[164] Diamant *et al.* have found that nanoporous $SrTiO_3$-coated TiO_2 electrodes improve the open circuit photovoltage while reducing the short circuit photocurrent, resulting in a 15% improvement in the DSSC conversion efficiency.[155]

3.3.3 Metal doping. Metal doping in nano-TiO_2 improves the conversion efficiency of DSSCs.[166–168] It is related to the electrical surface-state modification induced by metal doping. The doping process leads to significant changes in powder aggregation, charge transfer dynamics, and dye adsorption. As reported by Jeong *et al.*, a TiO_2 nanocrystalline film used in conventional DSSCs is modified in a $AgNO_3$–EtOH solution to adsorb 3 to 8 nm Ag nanoparticles (Fig. 17).[169] Compared to the 7.1% efficiency obtained from the cell without Ag nanoparticles, Ag doping improves the efficiency by 25% (to 8.9%) as a result of the surface plasmon resonance (SPR) effect stemming from the Ag nanoparticles. SPR generated by the metal nanoparticles enhances the optical absorption by the solar cell films by either generating light scattering to prolong the optical pathway or causing a local field enhancement to improve the optical absorption cross-section of the dye.[169] The optimal size of Ag nanoparticles is about 19 nm to enhance optical absorption by the dye-sensitized nano-TiO_2 film.[157] In practice, Ag nanoparticles with a size of over 19 nm may yield a more substantial SPR enhancement but the internal surface area of the photoelectrode film reduces, resulting in less adsorption and a decrease in the overall conversion efficiency.[170]

Su *et al.* have recently proposed a promising plasmonic solar cell.[171] The photoelectrode is composed of TiO_2 nanoparticles with 6 nm Au nanoparticles to serve as the sensitizer for light harvesting (Fig. 18a). The optical absorption of the Au-adsorbed TiO_2 film is proportional to the amount of adsorbed Au nanoparticles (Fig. 18b). The efficiency of the photoelectrical conversion increases with the amount of Au nanoparticles, from 0.016% for 1 layer of Au nanoparticles to 0.75% for 5 layers of Au nanoparticles. Meanwhile, the short-circuit electrical current increases from 1.076 to 5.192 mA cm^{-2}, as shown in Fig. 18c. The photoexcited electrons near the surface of the Au nanoparticles may have enough energy to overcome the Schottky barrier at the Au/TiO_2 interface and are injected into the conduction band of TiO_2 due to the SPR effect and overlap of the SPR absorption band.[171] Al and W doped nano-TiO_2 semiconducting powders have been incorporated into the working electrode of the DSSCs.[172] Ko *et al.* have observed that the Al-doped TiO_2 electrodes increase the open-circuit voltage (V_{oc}) but reduce the short-circuit current (J_{sc}). On the contrary, W-doped TiO_2 shows the opposite effects. The dual Al and W nanoparticle doped TiO_2 raises the DSSC efficiency on account of an enhanced photovoltage and photocurrent compared to the undoped one (Fig. 19).[172] Ag and Au are the most common

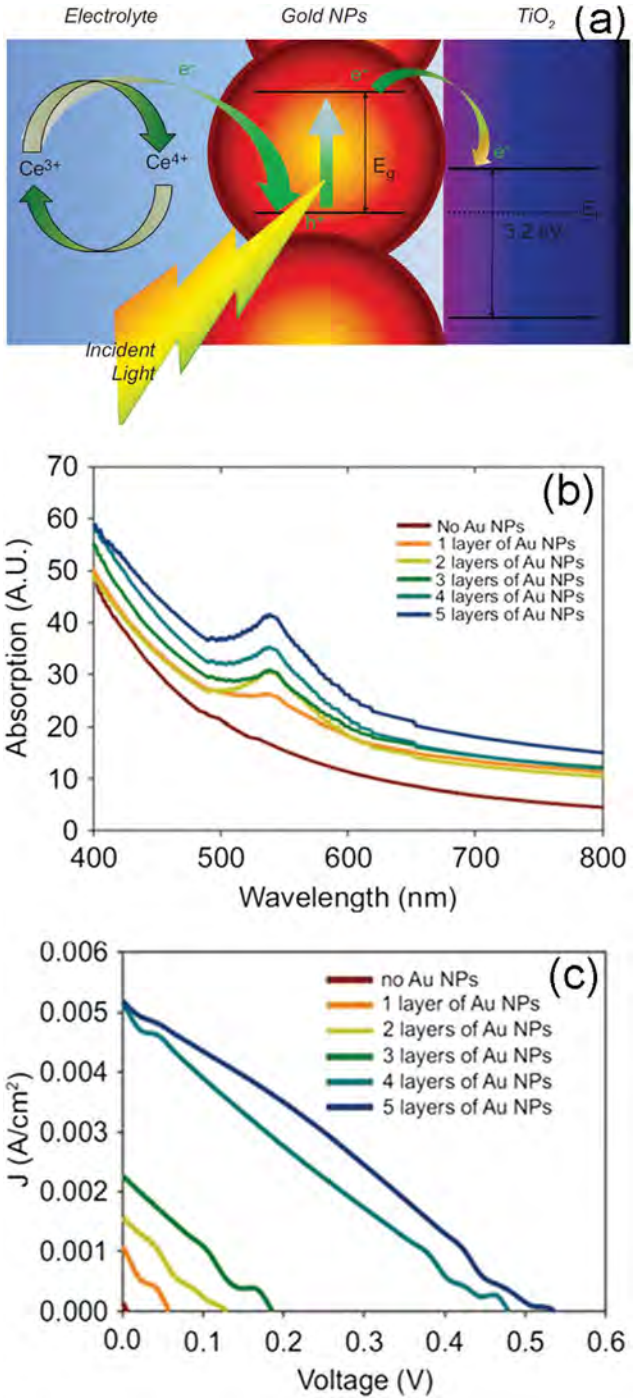

Fig. 18 Dye sensitized solar cell. (a) Schematic drawing showing SPR-induced electron injection from the metal nanoparticles to semiconductor, (b) optical absorption spectra of Au-adsorbed TiO_2 nanoparticle films, and (c) *I–V* curves of DSSCs with photoelectrode films consisting of TiO_2 nanoparticles adsorbed with different amounts of Au nanoparticles. Reprinted with permission from ref. 171.

metals that are used to enhance the optical absorption by solar cells, because they do not have many interband transitions, which may limit light absorption. Chou *et al.* have investigated the effects of Ag/Au addition.[173] A layer of TiO_2–Au (or TiO_2–Ag) composite particles is deposited on the FTO-glass substrate of the working electrode of a DSSC. With increasing Au (or Ag)

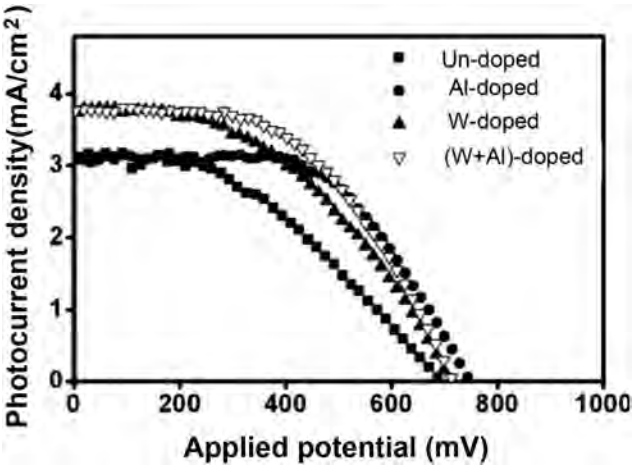

Fig. 19 Typical *I–V* characteristics of dye-sensitized solar cells under illumination. Reprinted with permission from ref. 172.

content in the composite particles, the conversion efficiency (η) of the DSSC increases. Furthermore, the η values of the DSSCs with a film of TiO_2–Au (or TiO_2–Ag) on the working electrode always exceed those of the conventional cells because of the Schottky barrier.[173]

3.4 Remarks

Nanostructured TiO_2 can improve the performance of solar cells due to their unique optical and/or electrical properties arising from their special structural characteristics. These optical or electrical properties can be utilized to either increase the optical absorption of the solar cells, or improve the electron transport in the solar cells. Therefore, it is essential to develop techniques or processes to optimize the structure, morphology, and photoelectrical conversion capability in order to further enhance the performance of DSSCs.

4. Nanostructured TiO_2 in fuel cells

A typical fuel cell is illustrated in Fig. 20.[174] According to the different types of electrolytes used, fuel cells can be divided into alkaline fuel cells (AFCs), proton exchange membrane fuel cells (PEMFCs), phosphoric acid fuel cells (PAFCs), molten carbonate fuel cells (MCFCs), and solid oxide fuel cells (SOFCs). The PEMFCs can further be subcategorized as hydrogen fuel cells and direct alcohol fuel cells (DAFCs). Because no hydrogen production is required by DAFCs, they have good prospects as convenient fuel sources in applications such as portable electronics, electrical vehicles, and chemical power sources. A DAFC is a proton exchange membrane fuel cell utilizing alcohol as the fuel, and theoretically, its specific energy density is larger than that of a LIB.[175] In addition, this type of cell has a simple structure, low working temperature, easy way to add fuel, and wider application to portable appliances. Recent research activities have mainly focused on direct methanol fuel cells (DMFCs) and direct ethanol fuel cells (DEFCs).[176,177]

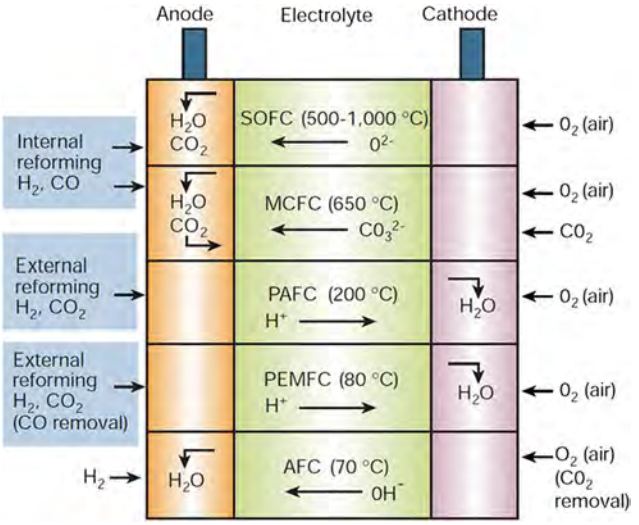

Fig. 20 Summary of fuel-cell types. Reprinted with permission from ref. 174.

4.1 Nanostructured TiO_2 in DAFCs

The slow kinetics and catalyst poisoning effect induced by CO have hampered the wide acceptance of DAFCs, but with a better understanding of the bifunctional mechanism, advanced electro-catalysts may solve these problems. Succinctly speaking, a second component like Ru can expedite the oxidation of CO to CO_2 and adsorb oxygen-containing species near the poisoned Pt sites.[163,164] It has been observed that transition metal oxides such as CeO_2, ZrO_2, and TiO_2 enhance the electro oxidation of alcohol on the surface of Pt and their good stability has caught the eyes of many researchers.[178–180] In fact, owing to its excellent photocatalytic ability, non-toxicity, and low price, TiO_2 is widely used in fuel cells and various forms of nano-TiO_2 are used as co-anode catalysts in DAFCs.[181–185]

4.1.1 Nanostructured TiO_2 as a catalyst carrier. Its high stability and resistance to acids and alkalis in conjunction with its large surface area render nanostructured TiO_2 a potential catalyst carrier. According to the bifunctional mechanism, the adsorbed hydroxyl groups on the oxide surface are transferred to the adjacent precious metal catalyst, thus accelerating the oxidation of these species and circumventing the catalyst poisoning effects. The active sites of the catalyst are thus released and the catalytic performance is improved.[186] The different forms of nano-TiO_2, for instance, nanotubes, nanorods, and nanobelts, influence the transfer effects. Guo *et al.* have used porous TiO_2 nanorods as carriers to obtain a new type of Pt/TiO_2 catalyst.[187] The Pt nanoparticles are uniformly loaded on the porous TiO_2 nanorods and the Pt/TiO_2 catalyst retains the porous structure which benefits the mass transfer during the methanol electro oxidation. Pd nanoparticles can also be scattered on the surface of TiO_2 nanotubes and used as a catalyst for methanol oxidation,[188] and compared to the use of pure Pd, this dispersion of Pd on TiO_2 nanotubes yields a better catalytic performance.

4.1.2 TiO_2 composite materials as the catalyst carrier. A good catalyst carrier in DAFCs requires not only good electrical conductivity, but also good proton performance.[189] A TiO_2–C composite carrier can satisfy these two requirements. Shim *et al.* have synthesized a Pt–TiO_2–C catalyst[190] and found that the performance of the composite catalyst is better than that of a Pt catalyst without TiO_2. Cyclic voltammograms reveal that the electrochemically active area on the Pt–TiO_2–C catalyst increases significantly. On account of oxidation, the ability of Pt to adsorb hydrogen and oxygen weakens. The catalytic improvement can be attributed to the interface between the Pt and oxide as well as the synergistic effects produced by the spread of the middle interface. Xiong *et al.* have fabricated a TiO_x/Pt/C catalyst[191] and both the synthesis method and subsequent heat treatment affect the catalytic activity. The TiO_x/Pt/C catalyst exhibits a higher catalytic activity and methanol resistance than the Pt/C catalyst because of the larger electrochemically active area, change of electronic properties, and enhanced resistance to methanol permeation.[191,192] Chen *et al.* have observed that addition of TiO_2 to the catalyst substrate benefits the dispersion of the Pt and Ru atoms on the cluster surface. The morphology of the catalyst is thus altered enabling dispersion of the catalyst in carbon.[193] By changing the TiO_2 content in the catalyst, the nanostructure can be tuned.[193] Mixed TiO_2 nanotubes have been incorporated into a Pt/C catalyst using an aqueous solution method to control ethanol electro oxidation.[194] Song *et al.* have observed that TiO_2 nanotubes enhance the utilization rate of Pt and the activity of the ethanol oxidation. CO stripping experiments reveal that the TiO_2 nanotubes reduce the CO oxidation peak potential and promote ethanol oxidation.[194] Further experiments disclosed that water in the TiO_2 nanotubes plays an important role in the improvement of the co-catalytic properties.[195]

4.2 Photocatalytic properties of TiO_2 in DMFC applications

A hybrid carbon fiber electrode comprising of a TiO_2 semiconductor photocatalyst and Pt–Ru catalyst has been developed to boost the performance of a direct methanol fuel cell (DMFC) as shown in Fig. 21.[196] TiO_2 can improve the performance of the Pt–Ru catalyst in darkness. Incorporation of this photocatalyst provides a new way to minimize the content of the precious metal and enhance the performance of DMFCs. At a low catalyst loading of 0.15 mg cm^{-2} at 295 K, a 25% enhancement in the peak power density is attained during light illumination. Park *et al.* have used Pt and TiO_2 targets to produce nanostructured Pt–TiO_2 electrodes with sputter deposition.[197] The efficiency of methanol oxidation is improved by 30% in the presence of ultraviolet light compared to the situation without light. This is ascribed to the photo-produced holes in TiO_2 under UV light illumination resulting in enhanced oxidation of methanol. Chu *et al.* have fabricated a nanoporous TiO_2 membrane based anode catalyst by the sol–gel method.[198] Pt/Ni/Ru nanoparticles (atomic ratio = 1 : 1 : 1) are deposited onto the TiO_2 nanoporous membrane by electrodeposition. By using the Pt–Ni–Ru/TiO_2 catalyst, the current density of ethanol oxidation is 2.5 times higher with sunlight compared to that without light due to the large number of stimulated photo-produced holes in this catalyst.[198]

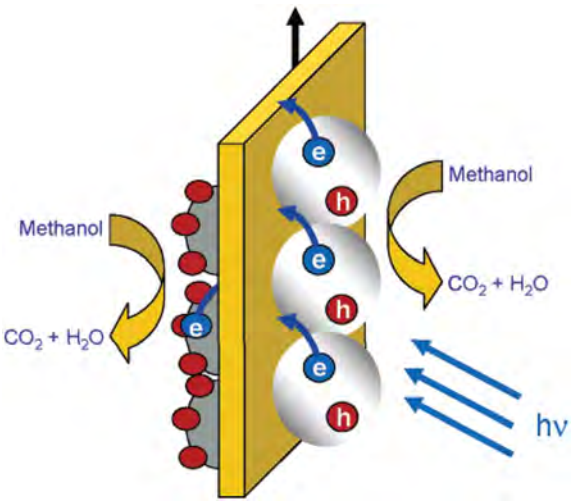

Fig. 21 Catalytic and photocatalytic oxidation of methanol on a Pt–Ru and TiO_2 modified carbon fiber electrode. Reprinted with permission from ref. 196.

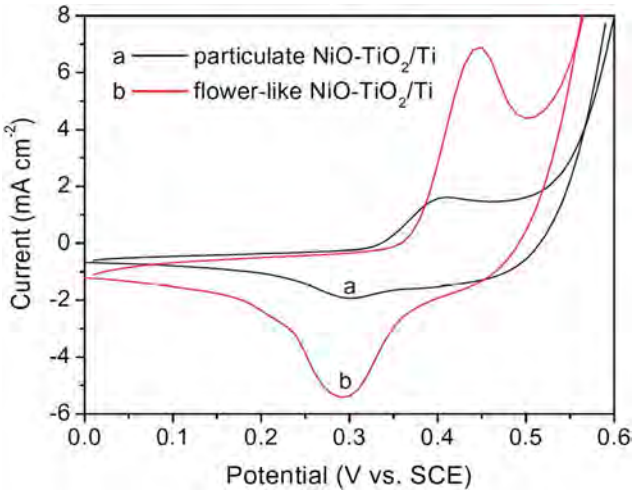

Fig. 22 Cyclic voltammetry measurement of particulate and flower-like NiO–TiO_2/Ti nanotube array composites in 1.0 M NaOH at a scanning rate of 5 mV s^{-1}. Reprinted with permission from ref. 231.

5. Nanostructured TiO_2 in supercapacitors

5.1 Introduction to supercapacitors

As energy storage devices, supercapacitors have attracted growing interests in recent years.[199–204] According to the mechanism governing charge storage, supercapacitors can be classified as electrical double layer capacitors (EDLCs) that are based on electrostatic charge diffusion and accumulation at the electrode–electrolyte interface and pseudocapacitors that are dominated by Faradaic reactions on the electrodes.[205–207] The limited charge accumulation in the electrical double layer restricts the specific capacitance of EDLCs in a relatively small range between 90 and 250 F g^{-1}. On the contrary, pseudocapacitors made of metal oxides or conducting polymers have higher specific capacitances of 300–1200 F g^{-1} *via* surface redox reactions.[208–214]

There are two common ways to enhance the electrochemical capacitance and stability of an electrode. The first way is to adopt a nanostructured electrode with a very large effective area. It has been demonstrated that nanostructures such as nanotubes, nanowires, nanosheets, and mesoporous nanostructures have higher specific capacitances than their bulk counterparts.[211–218] The second technique is to increase the electrical conductivity of the electrode by introducing conductive materials. For example, carbon materials as excellent electrical conductors have been used to form composites with metal oxide electrodes.[217–220] Recently, nanostructured TiO_2 has been used to fabricate supercapacitor electrodes due to the semiconducting properties, large accessible surface, and long-term chemical stability.[221–226]

5.2 Approaches to enhance electrochemical performance

5.2.1 Nanostructured TiO_2 electrodes. Besides its excellent semiconducting properties, nanostructured TiO_2 boasts nanoscale dimensions with a highly defined geometry and large surface area. It is thus suitable for electrochemical capacitors. Salari *et al.* have synthesized self-organized TiO_2 nanotubes and nanocrystalline TiO_2 powders[221,225] and the aligned TiO_2 nanotubes (TiO_2-NT) fabricated on the Ti substrate serve as the working electrode. The electrode shows exceptionally high values compared to the conventional TiO_2 electrode in supercapacitor applications.

5.2.2 Composite TiO_2 nanotubes as electrodes. TiO_2 nanotube arrays possess distinct advantages such as the provision of rigid tubular channels as well as a large number of active surface sites for redox reactions, ion diffusion, and charge transfer. These benefits, which have been discussed from the perspectives of rechargeable lithium batteries also apply to electrochemical supercapacitors.[227] Incorporation of TiO_2 nanotubes into metallic oxides or hydrous oxides can improve the performance of these compounds because of the better dispersion of the metal oxides or hydrous oxides and subsequently have better utilization. Wang *et al.* have used TiO_2 nanotubes as a solid support to disperse metal oxides.[228,229] A new composite composed of $Co(OH)_2$ and TiO_2 nanotubes has been synthesized by chemical precipitation[230] and the electrochemical capacitance determined by cyclic voltammetry and charging–discharging tests shows a maximum specific value of 229 F g^{-1}. The TiO_2 nanotubes supply a three-dimensional network for the composite enabling the homogeneous dispersion of $Co(OH)_2$ resulting in enhanced utilization.[230] Superior capacitance performance and larger energy density can be achieved from tailored NiO–TiO_2/Ti composites based on the encapsulation and microstructure modification of electroactive NiO.[231] Electroactive NiO incorporated into TiO_2 nanotubes grows from the inner wall to the top surface leaving an open pore mouth. The flower-like nanocomposite retains 92.3% of the initial capacitance after 1000 cycles and shows a good stability in the continuous charging–discharging process, as shown in Fig. 22.[231] This superior energy storage performance can be attributed to the highly accessible redox reaction sites on the three-dimensional NiO on the TiO_2 nanotubes.[231]

6. Conclusion and outlook

This review summarizes recent progress pertaining to the use of nanostructured TiO_2 in four important energy-related applications: lithium-ion batteries, dye-sensitized solar cells (DSSCs), fuel cells, and supercapacitors. Nanostructured TiO_2 enhances the performance of these devices due to its unique geometrical characteristics as well as its optical and electronic properties. Although the benefits of TiO_2 nanomaterials have been extensively reported, more insightful understanding of the relationship between the performance of energy-conversion/storage devices and the TiO_2 nanostructure is needed and must be studied further. New mechanisms associated with the TiO_2 nanostructure will be discovered and the knowledge will increase optical absorption properties while reducing charge recombination. At the same time, it is important to develop new structures. For example, in lithium-ion batteries, optimized structures can lead to more efficient intercalation–deintercalation and cycling stability of Li ions simultaneously. With regard to supercapacitors, TiO_2-based composite materials can deliver a high storage density at a low cost. All in all, in energy conversion/storage applications, the synthesis of appropriate nanomaterials continues to pose challenges because the device performance is related to the specific characteristics of the nanostructured TiO_2 such as surface morphology, structure, and surface chemistry.

Acknowledgements

This work is jointly supported by City University of Hong Kong Applied Research Grant (ARG) no. 9667066 and 9667069, National Natural Science Foundation of China no. 50901032, 51101053, and 81271715, as well as project of Excellent Scientist Fund in Hubei.

References

1 A. Fujishima and K. Honda, *Nature*, 1972, **37**, 238.
2 A. Fujishima, T. N. Rao and D. A. Tryk, *J. Photochem. Photobiol., C*, 2000, **1**, 1.
3 D. A. Tryk, A. Fujishima and K. Honda, *Electrochim. Acta*, 2000, **45**, 2363.
4 D. Li, H. Haneda, S. Hishita and N. Ohashi, *Chem. Mater.*, 2005, **17**, 2596.
5 M. R. Hoffmann, S. T. Martin, W. Choi and D. W. Bahnemann, *Chem. Rev.*, 1995, **95**, 69.
6 J. M. Ball, N. K. S. Davis and J. D. Wilkinson, *RSC Adv.*, 2012, **2**, 6846.
7 F. Zhu, D. Wu and Q. Li, *RSC Adv.*, 2012, **2**, 11629.
8 B. O'Regan and M. Gratzel, *Nature*, 1991, **353**, 737.
9 A. P. Alivisatos, *Science*, 1996, **271**, 933.
10 C. Burda, X. Chen, R. Narayanan and M. A. El-Sayed, *Chem. Rev.*, 2005, **105**, 1025.
11 C. B. Murray, C. R. Kagan and M. G. Bawendi, *Annu. Rev. Mater. Sci.*, 2000, **30**, 545.
12 Y. Yin and A. P. Alivisatos, *Nature*, 2005, **437**, 664.
13 T. Xia, M. Kovochich, J. Brant, M. Hotze, J. Sempf, T. Oberley, C. Sioutas, J. I. Yeh, M. R. Wiesner and A. E. Nel, *Nano Lett.*, 2006, **6**, 1794.
14 R. Zhang, Y. Niu, Y. Li, C. Zhao, B. Song, Y. Li and Y. Zhou, *Environ. Toxicol. Pharmacol.*, 2010, **30**, 52.
15 M. Ghosh, M. Bandyopadhyay and A. Mukherjee, *Chemosphere*, 2010, **81**, 1253.
16 S. Xiong, S. George, Z. Ji, S. Lin, H. Yu, R. Damoiseaux, B. France, K. W. Ng and S. C. J. Loo, *Arch. Toxicol.*, 2013, **87**, 99.
17 E. F. Chassot, V. Raspal, Y. Sibaud, O. K. Awitor, F. Bonnemoy, J. L. Bonnet and J. Bohatier, *Thin Solid Films*, 2011, **519**, 2564.
18 R. S. Dibbell, G. R. Soja, R. M. Hoth and D. F. Watson, *Langmuir*, 2007, **23**, 3432.
19 Y. Zhao, X. Zhang, J. Zhai, J. He, L. Jiang, Z. Liu, S. Nishimoto, T. Murakami, A. Fujishima and D. Zhu, *Appl. Catal., B*, 2008, **83**, 24.
20 M. Ye, J. Gong, Y. Lai, C. Lin and Z. Lin, *J. Am. Chem. Soc.*, 2012, **134**, 15720.
21 R. R. Djenadic, L. M. Nikolic, K. P. Giannakopoulos, B. Stojanovic and V. V. Srdic, *J. Eur. Ceram. Soc.*, 2007, **27**, 4339.
22 D. Cahen, G. Hodes, M. Graetzel, J. F. Guillemoles and I. Riess, *J. Phys. Chem. B*, 2000, **104**, 2053.
23 N. Robertson, *Angew. Chem., Int. Ed.*, 2006, **45**, 2338.
24 G. P. Wang, L. Zhang and J. J. Zhang, *Chem. Soc. Rev.*, 2012, **41**, 797.
25 J. Fernandez, S. Tennison, O. Kozynchenko, F. Rubiera, F. Stoeckli and T. Centeno, *Carbon*, 2009, **47**, 1598.
26 S. Ko, C. K. Banerjee and J. Sankar, *Composites, Part B*, 2011, **42**, 579.
27 M. Liu, L. Piao, L. Zhao, S. Ju, Z. Yan, T. He, C. Zhou and W. Wang, *Chem. Commun.*, 2010, **46**, 1664.
28 R. Leary and A. Westwood, *Carbon*, 2011, **49**, 741.
29 K. Gao and S. Li, *Appl. Surf. Sci.*, 2012, **258**, 6460.
30 T. K. Ghoraia, M. Chakraborty and P. Pramanik, *J. Alloys Compd.*, 2011, **509**, 8158.
31 J. S. Chen, L. A. Archer and X. W. Lou, *J. Mater. Chem.*, 2011, **21**, 9912.
32 J. Wang, Y. Zhou, Y. Hu, R. O'Hayre and Z. Shao, *J. Phys. Chem. C*, 2011, **115**, 2529.
33 T. Beuvier, M. R. Plouet, M. M. L. Granvalet, T. Brousse, O. Crosnier and L. Brohan, *Inorg. Chem.*, 2010, **49**, 8457.
34 Y. Ren, Z. Liu, F. Pourpoint, A. R. Armstrong, C. P. Grey and P. G. Bruce, *Angew. Chem.*, 2012, **124**, 2206.
35 J. W. Xu, C. H. Jia, B. Cao and W. F. Zhang, *Electrochim. Acta*, 2007, **52**, 8044.
36 H. Kim, R. C. Y. Auyeung, M. Ollinger, G. P. Kushto, Z. H. Kafafi and A. Piqué, *Appl. Phys. A: Mater. Sci. Process.*, 2006, **83**, 73.
37 C. Shena, Z. Q. Maa, L. Shena, L. Zhaoa, F. Xua, Y. H. Lia, Z. X. Zhao, F. Hong and W. Wu, *Integr. Ferroelectr.*, 2011, **128**, 130.
38 C. J. Lin, W. Y. Yu and S. H. Chien, *J. Mater. Chem.*, 2010, **20**, 1073.

39 P. Joshi, Y. Xie, M. Ropp, D. Galipeau, S. Bailey and Q. Qiao, *Energy Environ. Sci.*, 2009, **2**, 426.
40 W. Guo, C. Xu, X. Wang, S. Wang, C. Pan, C. Lin and Z. L. Wang, *J. Am. Chem. Soc.*, 2012, **134**, 4437.
41 M. Y. Song, D. K. Kim, K. J. Ihn, S. M. Jo and D. Y. Kim, *Synth. Met.*, 2005, **153**, 77.
42 D. J. Guo, X. P. Qiu, L. Q. Chen and W. T. Zhu, *Carbon*, 2009, **47**, 1680.
43 L. Barbora, S. Acharya and A. Verma, *Macromol. Symp.*, 2009, **277**, 177.
44 M. Gustavsson, H. Ekstrom, P. Hanarp, L. Eurenius, G. Lindbergh, E. Olsson and B. Kasemo, *J. Power Sources*, 2007, **163**, 671.
45 Q. Wang, Z. Wen and J. H. Li, *Adv. Funct. Mater.*, 2006, **16**, 2141.
46 G. Wang, Z. Y. Liu, J. N. Wu and Q. Lu, *Mater. Lett.*, 2012, **71**, 120.
47 P. G. Bruce, B. Scrosti and J. M. Tarascon, *Angew. Chem., Int. Ed.*, 2008, **47**, 2930.
48 R. Q. Song and H. Coelfen, *CrystEngComm*, 2011, **13**, 1249.
49 M. Winter and R. J. Brodd, *Chem. Rev.*, 2004, **104**, 4245.
50 M. Winter, J. O. Besenhard, M. E. Spahr and P. Novak, *Adv. Mater.*, 1998, **10**, 725.
51 D. Deng, M. G. Kim, J. Y. Lee and J. Cho, *Energy Environ. Sci.*, 2009, **2**, 818.
52 J. H. Pan, X. Zhang, A. J. Du, D. D. Sun and J. O. Leckie, *J. Am. Chem. Soc.*, 2008, **130**, 11256.
53 G. R. Patzke, F. Krumeich and R. Nesper, *Angew. Chem., Int. Ed.*, 2002, **41**, 2446.
54 H. Yin, Y. Wada, T. Kitamura, S. Kambe, S. Murasawa, H. Mori, T. Sakata and S. Yanagida, *J. Mater. Chem.*, 2001, **11**, 1694.
55 Q. Chen, W. Zhou, G. Du and L. M. Peng, *Adv. Mater.*, 2002, **14**, 1208.
56 L. Kavan, M. Kalbac, M. Zukalova, I. Exnar, V. Lorenzen, R. Nesper and M. Graetzel, *Chem. Mater.*, 2004, **16**, 477.
57 H. Zhang, G. R. Li, L. P. An, T. Y. Yan, X. P. Gao and H. Y. Zhu, *J. Phys. Chem. C*, 2007, **111**, 6143.
58 Y. G. Guo, J. S. Hu and L. J. Wan, *Adv. Mater.*, 2008, **20**, 2878.
59 P. Balaya, A. J. Bhattacharyya, J. Jamnik, Y. F. Zhukovskii, E. A. Kotomin and J. Maier, *J. Power Sources*, 2006, **159**, 171.
60 Y. Liu, D. Liu, Q. Zhang, D. Yu, J. Liu and G. Cao, *Electrochim. Acta*, 2011, **56**, 2559.
61 J. S. Chen and X. W. Lou, *J. Power Sources*, 2010, **195**, 2905.
62 B. L. He, B. Dong and H. L. Li, *Electrochem. Commun.*, 2007, **9**, 425.
63 Y. G. Guo, Y. S. Hu, W. Sigle and J. Maier, *Adv. Mater.*, 2007, **19**, 2087.
64 J. S. Chen, Y. L. Tan, C. M. Li, Y. L. Cheah, D. Y. Luan, S. Madhavi, F. Y. C. Boey, L. A. Archer and X. W. Lou, *J. Am. Chem. Soc.*, 2010, **132**, 6124.
65 G. N. Zhu, Y. G. Wang and Y. Y. Xia, *Energy Environ. Sci.*, 2012, **5**, 6652.
66 J. W. Fergus, *J. Power Sources*, 2010, **195**, 939.
67 K. Saravanan, K. Ananthanarayanan and P. Balaya, *Energy Environ. Sci.*, 2010, **3**, 939.
68 J. F. Ye, W. Liu, J. G. Cai, S. A. Chen, X. W. Zhao, H. H. Zhou and L. M. Qi, *J. Am. Chem. Soc.*, 2011, **133**, 933.
69 A. G. Dylla, J. A. Lee and K. J. Stevenson, *Langmuir*, 2012, **28**, 2897.
70 H. Zhou, D. Li, M. Hibino and I. Honma, *Angew. Chem., Int. Ed.*, 2005, **44**, 792.
71 M. Wagemaker, A. P. M. Kentgens and F. M. Mulder, *Nature*, 2002, **418**, 397.
72 G. Sudant, E. Baudrin, D. Larcher and J. M. Tarascon, *J. Mater. Chem.*, 2005, **15**, 1263.
73 J. P. Wang, Y. Bai, M. Y. Wu, J. Yin and W. F. Zhang, *J. Power Sources*, 2009, **191**, 614.
74 C. Jiang, I. Honma, T. Kudo and H. Zhou, *Electrochem. Solid-State Lett.*, 2007, **10**, A127.
75 Y. S. Hu, L. Kienle, Y. G. Guo and J. Maier, *Adv. Mater.*, 2006, **18**, 1421.
76 P. Kubiak, M. Pfanzelt, J. Geserick, U. Hörmann, N. Hüsing, U. Kaiser and M. W. Mehrens, *J. Power Sources*, 2009, **194**, 1099.
77 D. Wang, D. Choi, Z. Yang, V. V. Viswanathan, Z. Nie, C. Wang, Y. Song, J. G. Zhang and J. Liu, *Chem. Mater.*, 2008, **20**, 3435.
78 H. L. Fei and M. D. Wei, *Electrochim. Acta*, 2011, **56**, 6997.
79 A. R. Armstrong, G. Armstrong, J. R. Garcia and P. G. Bruce, *Adv. Mater.*, 2005, **17**, 862.
80 C. G. Nie, Z. L. Gong, L. Sun, J. Zuo, Y. K. Lai and C. J. Lin, *Electrochemistry*, 2004, **10**, 330.
81 S. M. Dong, H. B. Wang, L. Gu, X. H. Zhou, Z. H. Liu, P. X. Han, Y. Wang, X. Chen, G. L. Cui and L. Q. Chen, *Thin Solid Films*, 2011, **519**, 5978.
82 Y. Ren, Z. Liu, F. Pourpoint, A. R. Armstrong, C. P. Grey and P. G. Bruce, *Angew. Chem.*, 2012, **124**, 2206.
83 H. Han, T. Song, J. Y. Bae, L. F. Nazar, H. Kim and U. Paik, *Energy Environ. Sci.*, 2011, **4**, 4532.
84 W. H. Ryu, D. H. Nam, Y. S. Ko, R. H. Kim and H. S. Kwon, *Electrochim. Acta*, 2012, **61**, 19.
85 M. C. Yang, Y. Y. Lee, B. Xu, K. Powers and Y. S. Meng, *J. Power Sources*, 2012, **207**, 166.
86 Z. W. Seh, W. Li, J. J. Cha, G. Zheng, Y. Yang, M. T. McDowell, P. Hsu and Y. Cui, *Nat. Commun.*, 2013, **4**, 1.
87 P. I. Sorantin and K. Schwarz, *Inorg. Chem.*, 1992, **31**, 567.
88 T. Umebayashi, T. Yamaki, H. Itoh and K. Asai, *J. Phys. Chem. Solids*, 2002, **63**, 1909.
89 F. Gracia, J. P. Holgado, A. Caballero and A. R. Gonzalez-Elipe, *J. Phys. Chem. B*, 2004, **108**, 17466.
90 Y. Cao, W. S. Yang, W. F. Zhang, G. Z. Liu and P. Yue, *New J. Chem.*, 2004, **28**, 218.
91 A. Kubacka, G. Colon and M. F. Garcia, *Catal. Today*, 2009, **143**, 286.
92 T. Lindgren, J. Lu, A. Hoel, C. G. Granqvist, G. R. Torres and S. E. Lindquist, *Sol. Energy Mater. Sol. Cells*, 2004, **84**, 145.
93 H. Tian, J. F. Ma, K. Li and J. J. Li, *Mater. Chem. Phys.*, 2008, **112**, 47.
94 H. G. Jung, C. S. Yoon, J. Prakash and Y. K. Sun, *J. Phys. Chem. C*, 2009, **113**, 21258.

95 T. Bak, M. K. Nowotny, L. R. Sheppard and J. Nowotny, *J. Phys. Chem. C*, 2008, **112**, 7255.
96 M. M. Rahman, J. Z. Wang, D. Wexler, Y. Y. Zhang, X. J. Li, S. L. Chou and H. K. Liu, *J. Solid State Electrochem.*, 2010, **14**, 571.
97 S. H. Nam, H. S. Shim, Y. S. Kim, M. A. Dar, J. G. Kim and W. B. Kim, *ACS Appl. Mater. Interfaces*, 2010, **2**, 2046.
98 B. T. Zhao, R. Cai, S. M. Jiang, Y. J. Sha and Z. P. Shao, *Electrochim. Acta*, 2012, **85**, 636.
99 W. Wang, Q. Sa, J. Chen, Y. Wang, H. Jung and Y. Yin, *ACS Appl. Mater. Interfaces*, 2013, **5**, 6478.
100 X. Su, Q. Wu, X. Zhan, J. Wu, S. Wei and Z. Guo, *J. Mater. Sci.*, 2012, **47**, 2519.
101 D. Cai, P. Lian, X. Zhu, S. Liang, W. Yang and H. Wang, *Electrochim. Acta*, 2012, **74**, 65.
102 S. G. Lee, H. Deng, J. Hu, L. Zhou and H. Liu, *Int. J. Electrochem. Sci.*, 2013, **8**, 2204.
103 S. Liu, Z. Wang, C. Yu, H. B. Wu, G. Wang, Q. Dong, J. Qiu, A. Eychmüller and X. W. Lou, *Adv. Mater.*, 2013, **25**, 3462.
104 X. Wang, Q. Xiang, B. Liu, L. Wang, T. Luo, D. Chen and G. Shen, *Sci. Rep.*, 2007, **3**, 1.
105 M. Mancini, F. Nobili, R. Tossici, M. W. Mehrens and R. Marassi, *J. Power Sources*, 2011, **196**, 9665.
106 G. W. Crabtree and N. S. Lewis, *Phys. Today*, 2007, **60**, 37.
107 M. Gratzel, *Inorg. Chem.*, 2005, **44**, 6841.
108 R. E. H. Sims, *MRS Bull.*, 2008, **33**, 389.
109 M. A. Green, *Phys. Today*, 2004, **57**, 71.
110 K. W. J. Barnham, M. Mazzer and B. Clive, *Nat. Mater.*, 2006, **5**, 161.
111 H. Yu, S. Zhang, H. Zhao, G. Will and P. Liu, *Electrochim. Acta*, 2009, **54**, 1319.
112 P. Wang, S. M. Zakeeruddin, P. Comte, I. Exnar and M. Grätzel, *J. Am. Chem. Soc.*, 2003, **125**, 1166.
113 S. Alex, U. Santhosh and S. Das, *J. Photochem. Photobiol., A*, 2005, **172**, 63.
114 P. M. Sommeling, B. C. O'Regan, R. R. Haswell, H. J. P. Smit, N. J. Bakker, J. J. T. Smits, J. M. Kroon and J. A. M. van Roosmalen, *J. Phys. Chem. B*, 2006, **110**, 19191.
115 B. C. O'Regan, J. R. Durrant, P. M. Sommeling and N. J. J. Bakker, *J. Phys. Chem. C*, 2007, **111**, 14001.
116 A. Hagfeldt, G. Boschloo, L. Sun, L. Kloo and H. Pettersson, *Chem. Rev.*, 2010, **110**, 6595.
117 M. Gratzel, *Progr. Photovolt.: Res. Appl.*, 2000, **8**, 171.
118 M. Gratzel, *J. Photochem. Photobiol., C*, 2003, **4**, 145.
119 M. Gratzel, *MRS Bull.*, 2005, **30**, 23.
120 G. Deo, A. M. Turek and I. E. Wachs, *Appl. Catal., A*, 1992, **91**, 27.
121 D. Dambournet, I. Belharouak and K. Amine, *Chem. Mater.*, 2010, **22**, 1173.
122 S. Ito, P. Liska, P. Comte, R. Charvet, P. Péchy, U. Bach, L. S. Mende, S. M. Zakeeruddin, A. Kay, M. K. Nazeeruddin and M. Grätzel, *Chem. Commun.*, 2005, 4351.
123 Z. P. Zhang, S. Ito, B. O'Regan, D. B. Kuang, S. M. Zakeeruddin, P. Liska, R. Charvet, P. Comte, M. K. Nazeeruddin, P. Pechy, T. Koyanagi, T. Mizuno and M. Gratzel, *Z. Phys. Chem.*, 2007, **221**, 319.
124 S. Hore, P. Nitz, C. Vetter, C. Prahl, M. Niggemann and R. Kern, *Chem. Commun.*, 2005, 2011.
125 J. Barbé, A. F. Thomson, E. C. Wang, K. McIntosh and K. Catchpole, *Prog. Photovoltaics*, 2012, **20**, 143.
126 S. Schattauer, B. Reinhold, S. Albrecht, C. Fahrenson, M. Schubert, S. Janietz and D. Neher, *Colloid Polym. Sci.*, 2012, **290**, 1843.
127 R. Chauhan, A. Kumar and R. P. Chaudhary, *J. Sol-Gel Sci. Technol.*, 2012, **61**, 585.
128 Y. Wan, B. Sun, W. Liu and C. Qi, *J. Sol-Gel Sci. Technol.*, 2012, **61**, 558.
129 T. Touam, L. Znaidi, D. Vrel, I. N. Kuznetsova, O. Brinza, A. Fischer and A. Boudrioua, *Coatings*, 2013, **3**, 49.
130 W. Q. Wu, B. X. Lei, H. S. Rao, Y. F. Xu, Y. F. Wang, C. Y. Su and D. B. Kuang, *Sci. Rep.*, 2013, **3**, 1.
131 I. T. Hsiao, M. D. Lu, Y. L. Tung and H. Teng, *J. Phys. Chem. C*, 2010, **114**, 15625.
132 T. Cao, Y. Li, C. Wang, C. Shao and Y. Liu, *Langmuir*, 2011, **27**, 2946.
133 J. Liao, L. Shi, S. Yuan, Y. Zhao and J. Fang, *J. Phys. Chem. C*, 2009, **113**, 18778.
134 J. Zhu, S. Wang, Z. Bian, S. Xie, C. Cai, J. Wang, H. Yang and H. Li, *CrystEngComm*, 2010, **12**, 2219.
135 Z. Jiang, F. Yang, N. Luo, B. T. T. Chu, D. Sun, H. Shi, T. Xiao and P. P. Edward, *Chem. Commun.*, 2008, 6372.
136 S. Anandan and M. Ashokkumar, *Ultrason. Sonochem.*, 2009, **16**, 316.
137 C. Yu, J. C. Yu and M. Chan, *J. Solid State Chem.*, 2009, **182**, 1061.
138 J. Shi and X. Wang, *Cryst. Growth Des.*, 2011, **11**, 949.
139 N. T. Q. Hoa, Z. Lee and E. T. Kim, *Mater. Lett.*, 2012, **81**, 20.
140 D. Negrea, C. Ducu, S. Moga, V. Malinovschi, C. J. Monty, B. Vasile, D. Dorobantu and M. Enachescu, *J. Nanosci. Nanotechnol.*, 2012, **12**, 8746.
141 L. G. Garcia, G. Lozano, A. Barranco, H. Miguez and A. R. G. Elipe, *J. Mater. Chem.*, 2010, **20**, 6408.
142 S. Hore, E. Palomares, H. Smit, N. J. Bakker, P. Comte, P. Liska, K. R. Thampi, J. M. Kroon, A. Hinsch and J. R. Durrant, *J. Mater. Chem.*, 2005, **15**, 412.
143 Y. Lee, J. Chae and M. Kang, *J. Ind. Eng. Chem.*, 2010, **16**, 609.
144 Q. F. Zhang and G. Z. Cao, *Nano Today*, 2011, **6**, 91.
145 Q. Zhang, C. S. Dandeneau, X. Zhou and G. Cao, *Adv. Mater.*, 2009, **21**, 4087.
146 Q. Zhang, S. Yodyingyong, J. Xi, D. Myers and G. Cao, *Nanoscale*, 2012, **4**, 1436.
147 J. Kroon, N. Bakker, H. Smit, P. Liska, K. Thampi, P. Wang, S. Zakeeruddin, M. Gratzel, A. Hinsch and S. Hore, *Progr. Photovolt.: Res. Appl.*, 2007, **15**, 1.
148 A. Yella, H. W. Lee, H. N. Tsao, C. Yi, A. K. Chandiran, M. K. Nazeeruddin, E. W. G. Diau, C. Y. Yeh, S. M. Zakeeruddin and M. Gratzel, *Science*, 2011, **334**, 629.
149 V. Dhas, S. Muduli, S. Agarkar, A. Rana, B. Hannoyer, R. Banerjee and S. Ogale, *Sol. Energy*, 2011, **85**, 1213.
150 S. Li, Y. Liu, G. Zhang, X. Zhao and J. Yin, *Thin Solid Films*, 2011, **520**, 689.
151 X. Pan, C. Chen, K. Zhu and Z. Fan, *Nanotechnology*, 2011, **22**, 235402.

152 K. Kalyanasundaram and M. Gratzel, *Coord. Chem. Rev.*, 1998, **77**, 347.
153 Y. Lee and M. Kang, *Mater. Chem. Phys.*, 2010, **122**, 284.
154 S. G. Chen, S. Chappel, Y. Diamant and A. Zaban, *Chem. Mater.*, 2001, **13**, 4629.
155 Y. Diamant, S. G. Chen, O. Melamed and A. Zaban, *J. Phys. Chem. B*, 2003, **107**, 1977.
156 Y. Diamant, S. Chappel, S. G. Chen, O. Melamed and A. Zaban, *Coord. Chem. Rev.*, 2004, **248**, 1271.
157 A. Kay and M. Gratzel, *Chem. Mater.*, 2002, **14**, 2930.
158 C. Nasr, P. V. Kamat and S. Hotchandani, *J. Phys. Chem. B*, 1998, **102**, 10047.
159 E. Palomares, J. N. Clifford, S. A. Haque, T. Lutz and J. R. Durrant, *J. Am. Chem. Soc.*, 2003, **125**, 475.
160 N. G. Park, M. G. Kang, K. M. Kim, K. S. Ryu, S. H. Chang, D. K. Kim, J. van de Lagemaat, K. D. Benkstein and A. J. Frank, *Langmuir*, 2004, **20**, 4246.
161 S. Chappel, S. G. Chen and A. Zaban, *Langmuir*, 2002, **18**, 3336.
162 F. Fabregat-Santiago, J. Garcia-Canadas, E. Palomares, J. N. Clifford, S. A. Haque, J. R. Durrant, G. Garcia-Belmonte and J. Bisquert, *J. Appl. Phys.*, 2004, **96**, 6903.
163 B. C. O'Regan, S. Scully, A. C. Mayer, E. Palomares and J. Durrant, *J. Phys. Chem. B*, 2005, **109**, 4616.
164 E. Palomares, J. N. Clifford, S. A. Haque, T. Lutz and J. R. Durrant, *Chem. Commun.*, 2002, 1464.
165 G. R. A. Kumara, M. Okuya, K. Murakami, S. Kaneko, V. V. Jayaweera and K. Tennakone, *J. Photochem. Photobiol., A*, 2004, **164**, 183.
166 Z. Han, J. Zhang, Y. Yu and W. Cao, *Mater. Lett.*, 2012, **70**, 193.
167 X. Zhang, F. Liu, Q. L. Huang, G. Zhou and Z. S. Wang, *J. Phys. Chem. C*, 2011, **115**, 12665.
168 S. Muduli, O. Game, V. Dhas, K. Vijayamohanan, K. A. Bogle, N. Valanoor and S. B. Ogale, *Sol. Energy*, 2012, **86**, 1428.
169 N. C. Jeong, C. Prasittichai and J. Hupp, *Langmuir*, 2011, **27**, 14609.
170 C. Photiphitak, P. Rakkwamsuk, P. Muthitamongkol, C. S. Kung and C. Thanachayanont, *Int. J. Photoenergy*, 2011, **2011**, 258635.
171 Y. H. Su, Y. F. Ke, S. L. Cai and Q. Y. Yao, *Light: Sci. Appl.*, 2012, **1**, 1.
172 K. H. Ko, Y. C. Lee and Y. J. Jung, *J. Colloid Interface Sci.*, 2005, **283**, 482.
173 C. Chou, R. Y. Yang, C. K. Yeh and Y. J. Lin, *Powder Technol.*, 2009, **194**, 95.
174 B. C. H. Steele and A. Heinzel, *Nature*, 2001, **414**, 345.
175 J. Liu and G. Sun, *Physics*, 2004, **33**, 79.
176 K. Y. Chan, J. Ding, J. W. Ren, S. A. Cheng and K. Y. Tsang, *J. Mater. Chem.*, 2004, **14**, 505.
177 A. Hamnett, *Catal. Today*, 1997, **38**, 445.
178 Y. X. Bai, J. J. Wu and J. Y. Xi, *Electrochem. Commun.*, 2005, **7**, 1087.
179 J. S. Wang, J. Y. Xi and Y. X. Bai, *J. Power Sources*, 2007, **164**, 555.
180 H. Q. Song, X. P. Qiu and F. H. Li, *Electrochim. Acta*, 2008, **53**, 3708.
181 C. Lamy, A. Lima and V. LeRhun, *J. Power Sources*, 2002, **105**, 283.
182 S. Surampudi, S. R. Narayanan, E. Vamos, H. Frank, G. Halpert and A. LaConti, *J. Power Sources*, 1994, **47**, 377.
183 C. Zhang, H. Yu, Y. Li, W. Song, B. Yi and Z. Shao, *Electrochim. Acta*, 2012, **80**, 1.
184 M. Choun, S. Chung, H. Jeon, S. Uhm and J. Lee, *Electrochem. Commun.*, 2012, **24**, 108.
185 K. W. Park and K. S. Seol, *Electrochem. Commun.*, 2007, **9**, 2256.
186 J. Y. Xi, J. S. Wang and L. H. Yu, *Chem. Commun.*, 2007, 1656.
187 X. Guo, D. J. Guo and X. P. Qiu, *J. Power Sources*, 2009, **194**, 281.
188 M. Wang, D. J. Guo and H. L. Li, *J. Solid State Chem.*, 2005, **178**, 1996.
189 L. Cao, F. Scheiba and C. Roth, *Angew. Chem., Int. Ed.*, 2006, **45**, 5315.
190 J. Shim, C. R. Lee and H. K. Lee, *J. Power Sources*, 2001, **102**, 172.
191 L. Xiong and A. Manthiram, *Electrochim. Acta*, 2004, **49**, 4163.
192 Y. L. Lam, C. W. Kan and C. W. M. Yuen, *Fibers Polym.*, 2010, **11**, 551.
193 J. M. Chen, L. S. Sarma and C. H. Chen, *J. Power Sources*, 2006, **159**, 29.
194 H. Q. Song, X. P. Qiu and X. X. Li, *J. Power Sources*, 2007, **170**, 50.
195 H. Q. Song, X. P. Qiu and D. J. Guo, *J. Power Sources*, 2008, **178**, 97.
196 K. Drew, G. Girishkumar and K. Vinodgopal, *J. Phys. Chem. B*, 2005, **109**, 11851.
197 K. W. Park, S. B. Han and J. M. Lee, *Electrochem. Commun.*, 2007, 1578.
198 D. B. Chu, S. X. Wang and P. Zheng, *ChemSusChem*, 2009, **2**, 171.
199 J. R. Miller and P. Simon, *Science*, 2008, **321**, 651.
200 D. W. Liu, B. B. Garcia, Q. F. Zhang, Q. Guo, Y. Y. Zhang, S. S. Sepehri and G. Z. Cao, *Adv. Funct. Mater.*, 2009, **19**, 1015.
201 G. Yu, L. Hu, M. Vosgueritchian, H. Wang, X. Xie, J. R. McDonough, X. Cui, Y. Cui and Z. N. Bao, *Nano Lett.*, 2011, **11**, 2905.
202 D. S. Yuan, J. X. Chen, J. H. Zeng and S. X. Tan, *Electrochem. Commun.*, 2008, **10**, 1067.
203 L. Chen, L. J. Sun, F. Luan, Y. Liang, Y. Li and X. X. Liu, *J. Power Sources*, 2010, **195**, 3742.
204 J. Bae, M. K. Song, Y. J. Park, J. M. Kim, M. Liu and Z. L. Wang, *Angew. Chem., Int. Ed.*, 2011, **50**, 1683.
205 P. Simon and Y. Gogotsi, *Nat. Mater.*, 2008, **7**, 845.
206 Y. R. Ahn, M. Y. Song, S. Jo, C. R. Park and D. Y. Kim, *Nanotechnology*, 2006, **17**, 2865.
207 X. Y. Lang, A. Hirata, T. Fujita and M. W. Chen, *Nat. Nanotechnol.*, 2011, **6**, 232.
208 C. C. Hu, K. H. Chang, M. C. Lin and Y. T. Wu, *Nano Lett.*, 2006, **6**, 2690.
209 P. C. Chen, H. T. Chen, J. Qiu and C. W. Zhou, *Nano Res.*, 2010, **3**, 594.

210 J. W. Lee, T. Ahn, J. H. Kim, J. M. Ko and J. D. Kim, *Electrochim. Acta*, 2011, **56**, 4849.

211 M. Jayalakshmi and K. Balasubramanian, *Int. J. Electrochem. Sci.*, 2008, **3**, 1196.

212 X. H. Lu, D. Z. Zheng, T. Zhai, Z. Q. Liu, Y. Y. Huang, S. L. Xie and Y. X. Tong, *Energy Environ. Sci.*, 2011, **4**, 2915.

213 C. C. Hu, H. Y. Guo, K. H. Chang and C. C. Huang, *Electrochem. Commun.*, 2009, **11**, 1631.

214 D. S. Yuan, T. X. Zhou, S. L. Zhou, W. J. Zou, S. S. Mo and N. N. Xia, *Electrochem. Commun.*, 2011, **13**, 242.

215 J. J. Xu, K. Wang, S. Z. Zu, B. H. Han and Z. X. Wei, *ACS Nano*, 2010, **4**, 5019.

216 Y. Gao, Y. S. Zhou, M. Qian, X. N. He, J. Redepenning, P. Goodman, H. M. Li, L. Jiang and Y. F. Lu, *Carbon*, 2013, **51**, 52.

217 A. D. Su, X. Zhang, A. Rinaldi, S. T. Nguyen, H. Liu, Z. Lei, L. Lu and H. M. Duong, *Chem. Phys. Lett.*, 2013, **561**, 68.

218 J. Yan, Z. Fan, T. Wei, W. Qian, M. Zhang and F. Wei, *Carbon*, 2010, **48**, 3825.

219 L. B. Hu, W. Chen, X. Xie, N. Liu, Y. Yang, H. Wu, Y. Yao, P. Mauro, H. N. Alshareef and Y. Cui, *ACS Nano*, 2011, **5**, 8904.

220 Y. Q. Dou, Y. P. Zhai, H. J. Liu, Y. Y. Xia, B. Tu, D. Y. Zhao and X. X. Liu, *J. Power Sources*, 2011, **196**, 1608.

221 M. Salari, S. H. Aboutalebi, K. Konstantinov and H. K. Liu, *Phys. Chem. Chem. Phys.*, 2011, **13**, 5038.

222 F. F. Santiago, H. Randriamahazaka, A. Zaban, J. G. Canadas, G. G. Belmontea and J. Bisquerta, *Phys. Chem. Chem. Phys.*, 2006, **8**, 1827.

223 H. T. Fang, M. Liu, D. W. Wang, T. Sun, D. S. Guan, F. Li, J. Zhou, T. K. Sham and H. M. Cheng, *Nanotechnology*, 2009, **20**, 225701.

224 Y. Xie, L. Zhou, C. Huang, H. Huang and J. Lu, *Electrochim. Acta*, 2008, **53**, 3643.

225 M. Salari, K. Konstantinov and H. K. Liu, *J. Mater. Chem.*, 2011, **21**, 5128.

226 B. Chen, J. B. Hou and K. Lu, *Langmuir*, 2013, **29**, 5911.

227 Y. K. Zhou, L. Cao, F. B. Zhang, B. L. He and H. L. Li, *J. Electrochem. Soc.*, 2003, **150**, A1246.

228 Y. G. Wang and X. G. Zhang, *J. Electrochem. Soc.*, 2005, **152**, A671.

229 Y. G. Wang and X. G. Zhang, *Electrochim. Acta*, 2004, **49**, 1957.

230 F. Tao, Y. Shen, Y. Liang and H. Li, *J. Solid State Electrochem.*, 2007, **11**, 853.

231 Y. Xie, C. Huang, L. Zhou, Y. Liu and H. Huang, *Compos. Sci. Technol.*, 2009, **69**, 2108.